Patterns of CO_2 and radiocarbon across high northern latitudes during International Polar Year 2008

S. A. Vay,[1] Y. Choi,[2] K. P. Vadrevu,[3] D. R. Blake,[4] S. C. Tyler,[4,5] A. Wisthaler,[6] A. Hecobian,[7] Y. Kondo,[8] G. S. Diskin,[1] G. W. Sachse,[2] J.-H. Woo,[9] A. J. Weinheimer,[10] J. F. Burkhart,[11] A. Stohl,[11] and P. O. Wennberg[12]

Received 15 January 2011; revised 27 March 2011; accepted 25 April 2011; published 16 July 2011.

[1] High-resolution in situ CO_2 measurements were conducted aboard the NASA DC-8 aircraft during the ARCTAS/POLARCAT field campaign, a component of the wider 2007–2008 International Polar Year activities. Data were recorded during large-scale surveys spanning the North American sub-Arctic to the North Pole from 0.04 to 12 km altitude in spring and summer of 2008. Influences on the observed CO_2 concentrations were investigated using coincident CO, black carbon, CH_3CN, HCN, O_3, C_2Cl_4, and $\Delta^{14}CO_2$ data, and the FLEXPART model. In spring, the CO_2 spatial distribution from 55°N to 90°N was largely determined by the long-range transport of air masses laden with Asian anthropogenic pollution intermingled with Eurasian fire emissions evidenced by the greater variability in the mid-to-upper troposphere. At the receptor site, the enhancement ratios of CO_2 to CO in pollution plumes ranged from 27 to 80 ppmv ppmv^{-1} with the highest anthropogenic content registered in plumes sampled poleward of 80°N. In summer, the CO_2 signal largely reflected emissions from lightning-ignited wildfires within the boreal forests of northern Saskatchewan juxtaposed with uptake by the terrestrial biosphere. Measurements within fresh fire plumes yielded CO_2 to CO emission ratios of 4 to 16 ppmv ppmv^{-1} and a mean CO_2 emission factor of 1698 ± 280 g kg^{-1} dry matter. From the ^{14}C in CO_2 content of 48 whole air samples, mean spring (46.6 ± 4.4‰) and summer (51.5 ± 5‰) $\Delta^{14}CO_2$ values indicate a 5‰ seasonal difference. Although the northern midlatitudes were identified as the emissions source regions for the majority of the spring samples, depleted $\Delta^{14}CO_2$ values were observed in <1% of the data set. Rather, ARCTAS $\Delta^{14}CO_2$ observations (54%) revealed predominately a pattern of positive disequilibrium (1–7‰) with respect to background regardless of season owing to both heterotrophic respiration and fire-induced combustion of biomass. Anomalously enriched $\Delta^{14}CO_2$ values (101–262‰) measured in emissions from Lake Athabasca and Eurasian fires speak to biomass burning as an increasingly important contributor to the mass excess in $\Delta^{14}CO_2$ observations in a warming Arctic, representing an additional source of uncertainty in the quantification of fossil fuel CO_2.

Citation: Vay, S. A., et al. (2011), Patterns of CO_2 and radiocarbon across high northern latitudes during International Polar Year 2008, *J. Geophys. Res.*, *116*, D14301, doi:10.1029/2011JD015643.

1. Introduction

[2] The Arctic and sub-Arctic regions of Alaska, Canada, and Greenland represent a vast wilderness with extremely low levels of human activity, one of the largest such land areas remaining in the world [*Wofsy et al.*, 1992]. Atmospheric composition over this region is regulated mainly by natural processes and by the long-range transport (LRT) of pollution that originates mostly from more southerly latitudes [*Gregory et al.*, 1992]. Nature and man have conspired to

[1]Chemistry and Dynamics Branch, NASA Langley Research Center, Hampton, Virginia, USA.
[2]National Institute of Aerospace, Hampton, Virginia, USA.
[3]Department of Geography, University of Maryland, College Park, Maryland, USA.
[4]Department of Chemistry, University of California, Irvine, California, USA.
[5]Chemistry Program, Norco College, Norco, California, USA.
[6]Institute for Ion Physics and Applied Physics, University of Innsbruck, Innsbruck, Austria.
[7]School of Earth and Atmospheric Sciences, Georgia Institute of Technology, Atlanta, Georgia, USA.
[8]Department of Earth and Planetary Science, University of Tokyo, Tokyo, Japan.
[9]Department of Advanced Technology Fusion, Konkuk University, Seoul, South Korea.
[10]Atmospheric Chemistry Division, National Center for Atmospheric Research, Boulder, Colorado, USA.
[11]Norwegian Institute for Air Research, Kjeller, Norway.
[12]Division of Geological and Planetary Sciences, California Institute of Technology, Pasadena, California, USA.

0148-0227/11/2011JD015643

make northern Eurasian sources far more available to the Arctic than those in North America [*Barrie*, 1986], though recent evidence suggests that contributions from rapidly developing economies in south Asia are gaining importance in the Arctic upper troposphere [*Koch and Hansen*, 2005]. Local pollution sources in the Arctic are currently small (e.g., volcanic emissions, conurbations, industrial emissions, the oil and shipping industry), and are limited to near the Arctic Circle [*Law and Stohl*, 2007].

[3] Glacial records signify that Arctic air pollution has undergone a marked increase since the mid 1950s paralleling accelerating CO_2 emissions [*Barrie*, 1986]. Accumulating observational evidence indicates a recent region-wide warming as a direct consequence of increasing levels of long-lived greenhouse gases and positive feedbacks specific to the region (e.g., sea ice albedo) [*Law and Stohl*, 2007; *Quinn et al.*, 2007]. Most observations of the Arctic atmosphere have been surface-based, yet contemporary studies reveal pollution influences are a year-round multialtitude phenomenon [*Klonecki et al.*, 2003; *Stohl*, 2006; *Shindell et al.*, 2008]. Synoptic weather systems, the primary transport mechanism, bring pollutants from distant industrial/urban and fire sources to the region predominately in winter and spring [*Fuelberg et al.*, 2010]. During summer, the influence of LRT is comparatively weak thus the composition of the atmosphere is most strongly affected by regional emissions, particularly boreal forest fires [*Gregory et al.*, 1992].

[4] While fossil fuel burning contributes significantly to the growth in atmospheric CO_2 levels, pyrogenic emissions are recognized as an additional source [*Crutzen and Andreae*, 1990], particularly at high northern latitudes where rising Arctic temperatures facilitate increased fire frequency [*Stocks et al.*, 1998]. Ecosystems within this northern expanse are comprised of interrelated habitats of forests, lakes, wetlands, rivers and tundra sequestering large carbon stocks in soils and permafrost [*Oechel and Vourlitis*, 1994] that are particularly vulnerable to a changing fire regime. Wildfire disturbance within boreal ecosystems represents a major perturbation to the Arctic atmosphere through the transfer of large amounts of terrestrial carbon to the atmosphere, approximately 89% in the form of CO_2 [*Stocks*, 1991]. Under a doubled CO_2 scenario, General Circulation Models project a 4°–6°C rise in summer temperatures with a commensurate decrease in soil moisture for much of Canada and Russia thereby increasing fire danger by 50% and lengthening the fire season by 30 days [*Goode et al.*, 2000]. More frequent and severe fires will have a significant impact on the age class structure of vegetation, the carbon budget, air quality, and climate of the boreal/Arctic zone in particular [*Kasischke and Bruhwiler*, 2002; *Soja et al.*, 2004; *Kasischke et al.*, 2005; *Paris et al.*, 2009] and the globe in general.

[5] As part of the wider Polar Study using Aircraft, Remote Sensing, Surface Measurements and Models, of Climate, Chemistry, Aerosols, and Transport (POLARCAT) executed during the 2007–2008 International Polar Year (IPY), NASA conducted the Arctic Research of the Composition of the Troposphere from Aircraft and Satellites (ARCTAS) mission in the spring and summer of 2008. An objective of ARCTAS was to better understand the factors driving current changes in Arctic atmospheric composition and climate through detailed observations of the chemical and radiative properties of gases and aerosols utilizing instrumented aircraft. An in-depth description of the ARCTAS mission, instrumentation, and first results is given by *Jacob et al.* [2010], while *Fuelberg et al.* [2010] provide a meteorological overview.

[6] This paper describes CO_2 and $\Delta^{14}CO_2$ measurements obtained over the North American Arctic and sub-Arctic during ARCTAS. In this study, we present the large-scale distributions of CO_2 and $\Delta^{14}CO_2$, showing the observed seasonal and spatial variability. We determine CO_2 to CO enhancement ratios in pollution plumes transported to the receptor region to quantify their impact on the composition of the Arctic atmosphere. Using a combination of gas-phase and aerosol-phase tracers in concert with the FLEXPART model, we then investigate the chemical characteristics of the plumes and transport pathways for source attribution. CO_2 emissions from wildfires within Canadian boreal forests are also examined. In the final section, contributions to the total measured CO_2 signal using $\Delta^{14}CO_2$ data are explored.

2. Deployment Strategy and Measurements

[7] The regional-scale coverage for the ARCTAS campaign is presented in Figure 1. The spring deployment (ARCTAS-A) was based out of Fairbanks, Alaska (65°N, 148°W) from 4 to 17 April 2008 and consisted of three local flights in addition to two round-trip flights to Thule, Greenland (77°N, 69°W). Rapidly deteriorating landing conditions in Thule required the DC-8 to divert to Iqaluit, Nunavut (64°N, 69°W) on 8 April. From 29 June through 10 July 2008 (ARCTAS-B), four local sorties were flown from the Cold Lake, Alberta (54°N, 110°W) summer base. There was also another flight to Thule for a two-night stay to overfly the Summit Greenland Observatory (73°N, 39°W).

[8] CO_2 mixing ratios were determined using a modified LI-COR model 6252 nondispersive infrared gas analyzer. This dual-cell instrument achieves high precision by measuring the differential absorption between ambient air and a calibrated reference gas traceable to the World Meteorological Organization primary CO_2 standards maintained by NOAA ESRL. The LI-COR-based CO_2 sampling system was operated at constant pressure (250 torr) and temperature (35°C) and had a precision of ±0.1 ppmv and accuracy of ±0.25 ppmv. Experimental procedures are described in detail by *Vay et al.* [2003]. The ARCTAS in situ CO_2 data are archived at 1 s resolution and are publically available via http://www-air.larc.nasa.gov. On 12 April, an in-flight intercomparison conducted over Alaska between the NASA DC-8 ARCTAS and the NOAA WP-3D Aerosol, Radiation, and Cloud Processes affecting Arctic Climate (ARCPAC) chemistry payloads showed no detectable difference between respective airborne in situ CO_2 instruments over a wide range of atmospheric conditions [*Peischl et al.*, 2010].

[9] The ^{14}C content of CO_2 ($\Delta^{14}CO_2$) was determined from air remaining in a select subset (n = 48) of whole air canister samples collected onboard the DC-8 for measurements of nonmethane volatile organic compounds (NMVOCs) [*Blake et al.*, 1996; *Simpson et al.*, 2010, 2011]. Postmission, measurements of the radiocarbon content on CO_2 were made at the W. M. Keck Carbon Isotope Accelerator Mass Spectrometer Facility at the University of CA-Irvine (UCI). Overall $\Delta^{14}C$ measurement precision is ±2‰ [*Tyler et al.*,

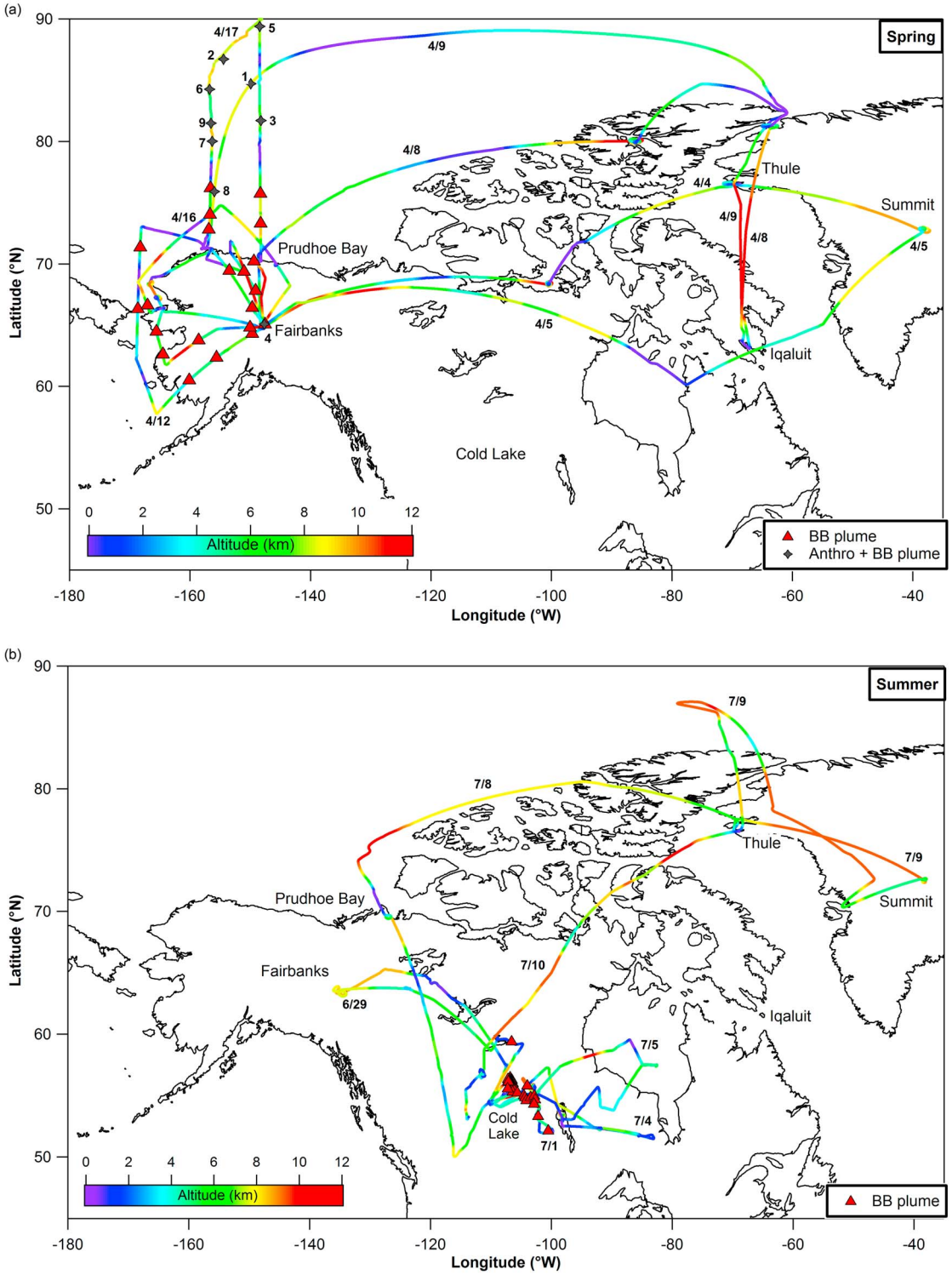

Figure 1. DC-8 flight tracks with sampling height and flight date. (a) ARCTAS-A with biomass burning (BB) and anthropogenic (Anthro) plume locations. (b) ARCTAS-B with fire plume locations.

1999; *Vay et al.*, 2009] where $\Delta^{14}C$ is defined by *Stuiver and Polach* [1977].

[10] In addition to CO_2 and $\Delta^{14}CO_2$, data from high-resolution in situ measurements of carbon monoxide (CO) [*Sachse et al.*, 1987]; black carbon (BC) [*Moteki and Kondo*, 2007; *Kondo et al.*, 2011]; acetonitrile (CH_3CN) [*Wisthaler et al.*, 2002]; hydrogen cyanide (HCN) [*Crounse et al.*, 2009]; and ozone (O_3) [*Weinheimer et al.*, 1994] are used in this study. We also utilize a number of NMVOC measurements obtained from whole air samples [*Blake et al.*,1996;

Table 1. DC-8-Based Observations Used in This Analysis

Compound	Formula	Precision	Accuracy (%)	Data Interval
Carbon monoxide	CO	1 ppbv	1	1 s
Black Carbon	BC	10%	10	60 s
Acetonitrile	CH_3CN	±30%[a]	±10	10 s
Hydrogen cyanide	HCN	5%	<±30	10 s
Ozone	O_3	<1 ppbv[b]	5	1 s
Tetrachloroethene	C_2Cl_4	1.2 pptv	10	variable
1,2-Dichloroethane	$C_2H_4Cl_2$	5 pptv	20	variable
Methyl chloride	CH_3Cl	1.5 pptv	5	variable
Carbonyl sulphide	OCS	2 pptv	10	variable
Propane	C_3H_8	0.7 pptv	5	variable
Benzene	C_6H_6	2 pptv	5	variable
Ethyl chloride	C_2H_5Cl	5%	30	variable
i-Pentane	C_5H_{12}	2 pptv	5	variable

[a]For 100 ppt ambient concentration.
[b]For tropospheric O_3 mixing ratios.

Simpson et al., 2010, 2011]. The measurement precision and accuracy of these compounds are given in Table 1.

3. Data and Methodology

[11] By definition, an emission ratio refers to fresh emissions, describing $\Delta X/\Delta Y$ at t = 0; whereas an enhancement ratio accounts for aging over a transport time Δt [*Lefer et al.*, 1994; *de Gouw et al.*, 2006]. Long-range transport of pollution to the Arctic during ARCTAS presented the opportunity to examine enhancement ratios for CO_2 relative to CO (CO_2:CO) providing insight into the CO_2 content of pollution plumes entering the Arctic (receptor site), and influencing the atmospheric composition of the region. CO is emitted by incomplete combustion, and we use it here as a tracer of pollution. Its atmospheric lifetime against oxidation by the hydroxyl radical (OH) is on average two months, long enough to track transport on intercontinental scales yet short enough to show well-defined concentration gradients [*Staudt et al.*, 2001; *Heald et al.*, 2003; *Yashiro et al.*, 2009].

[12] CO_2 and CO often share common combustion sources and are coemitted at specific ratios depending on the source and the combustion efficiency. Observationally based estimates of CO_2:CO are sensitive to all sources of CO_2 and CO that have statistical correlation and include both coemitting sources and adjacent but separate sources that become correlated because of transport [*Wang et al.*, 2010]. For example, in addition to its anthropogenic sources, CO_2 has a seasonally varying biospheric flux that can become correlated with other urban emissions when the urban plume is sampled downwind [*Vay et al.*, 2003; *Pataki et al.*, 2003; *Newman et al.*, 2008; *Wang et al.*, 2010]. Since ARCTAS-A occurred during early spring conditions in the Arctic and sub-Arctic, biological processes which produce CO_2 can be expected to be largely dormant, and the removal of CO_2 from the atmosphere by photosynthesis and dissolution in the oceans may be safely assumed to be minimal.

[13] Transport from lower latitudes to the Arctic can occur when surface emissions are rapidly lofted into the free troposphere by warm conveyor belts (WCBs) preceding surface cold fronts [*Liu et al.*, 2003; *Stohl*, 2006; *Fuelberg et al.*, 2010], or uplifted during transport because of the large latitudinal gradient in potential temperature [*Matsui et al.*, 2011]. Once in the free troposphere, these emissions-enriched air masses can preserve their identity as well-defined layers for a week or more as they are transported on intercontinental scales [*Rastigejev et al.*, 2010]. Some polluted air masses can travel long distances to the Arctic without species selective loss mechanisms changing their composition, while others may undergo CO oxidization by OH thus altering the CO_2:CO ratio characteristic of some distant source region from that observed at the receptor site [*Heard et al.*, 2004; *Campbell et al.*, 2007]. Though the composition of the pollution plumes may change during transport, it is their content upon arrival at the receptor site that inevitably influences the composition of the Arctic atmosphere. Recognizing this potential, we couple the comparison of the measured data to known emission ratios from specific source regions with concurrent tracer measurements, and data products from the Lagrangian particle dispersion model FLEXPART [*Stohl et al.*, 2002] rather than relying solely on the enhancement ratios to investigate influences on CO_2 spatial variability.

[14] CO_2:CO slopes for the plumes are obtained using orthogonal distance regression (ODR) fits [*Boggs et al.*, 1988] to the 1s data. Simultaneous tracer measurements with a wide range of lifetimes and sources are invoked to provide resolution of the relevant time scales for transport, and to characterize natural and anthropogenic emissions. Our analysis mainly relies on CO as a product of inefficient combustion; CH_3CN and HCN as indicators of biomass burning [*Li et al.*, 2000, 2003; *de Gouw et al.*, 2003]; BC produced only by incomplete combustion of carbonaceous materials [*Hansen and Novakov*, 1989]; and C_2Cl_4, a purely anthropogenic tracer released exclusively from industrial processes [*Blake et al.*, 1996, 1997]. Other chemical species data used in this study (Table 1) include i-pentane as a tracer of vehicular combustion and gasoline evaporation [*Blake and Rowland*, 1995; *Simpson et al.*, 2010]; propane (C_3H_8) as a probe for natural gas [*Katzenstein et al.*, 2003; *Harrigan et al.*, 2011]; and benzene (C_6H_6), a tracer of incomplete combustion [*Blake et al.*, 2003]. As an anthropogenic fingerprint for China, we invoke the suite of tracers 1,2-dichloroethene (1,2-DCE), methyl chloride (CH_3Cl), carbonyl sulfide (OCS), and ethyl chloride (C_2H_5Cl) [*Barletta et al.*, 2009]. Since the sources of these atmospheric trace species are predominately land-based, the impact of continental emissions on air masses can be assessed by the observed changes in their mixing ratios.

[15] To accommodate the different sampling frequencies of the many instruments on the DC-8, several time-base merges of the data were generated in which reported observations were averaged over specific intervals that include 10 s and 1 min. A separate merge was also generated for the whole air canister samples (UCI merge) which were typically collected over a 1 min period every 3–5 min during horizontal flight legs, and every 1–2 min during ascents, descents and plume encounters [*Simpson et al.*, 2010, 2011]. The data interval used for each tracer considered in this study is noted in Table 1.

4. Results and Discussion

4.1. Large-Scale CO_2 Distributions

[16] Figure 2 shows the CO_2 data for each ARCTAS deployment averaged at 0.5° latitude × 0.1 km altitude

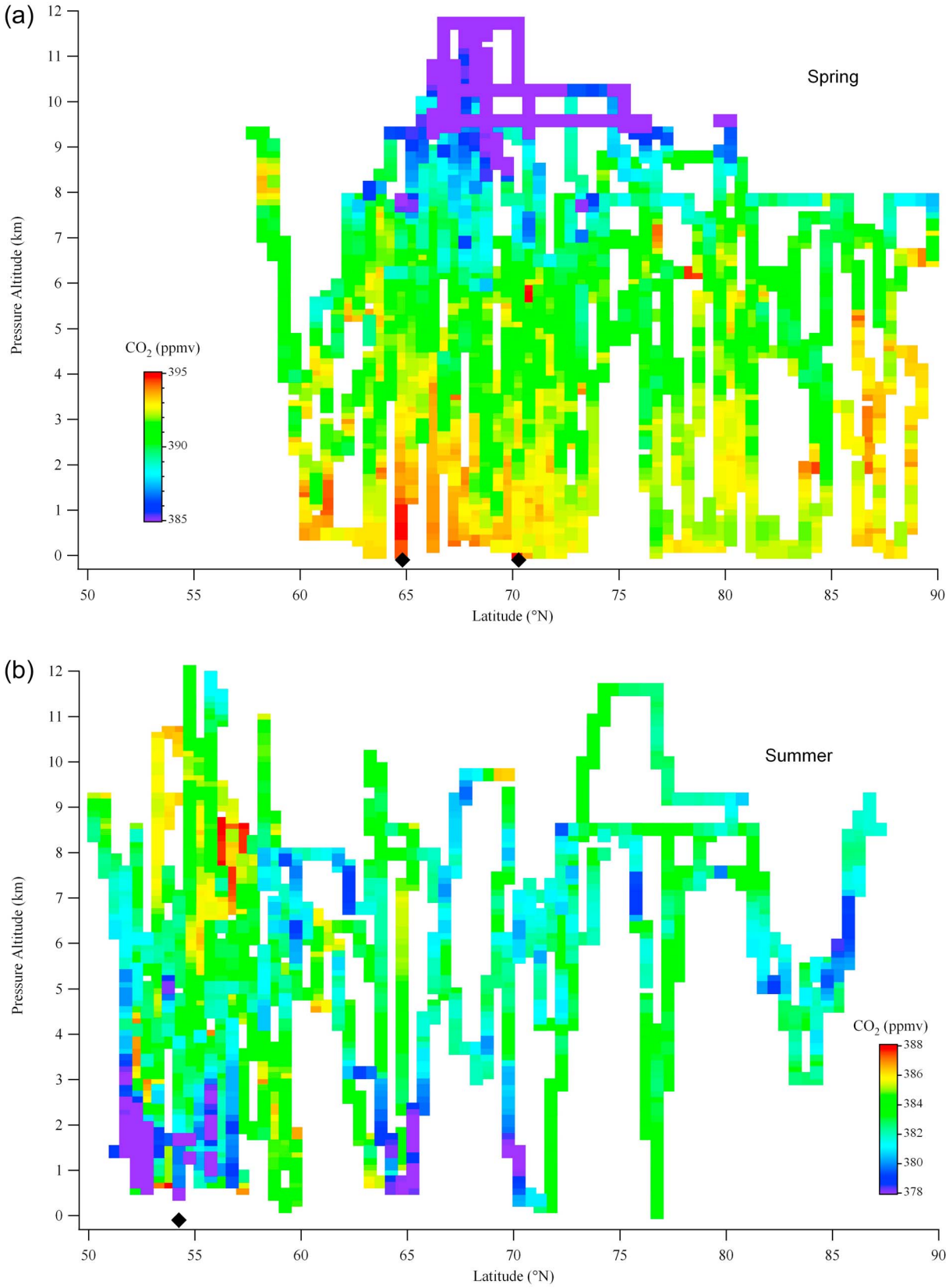

Figure 2. Large-scale distribution of CO_2 over the Arctic and sub-Arctic. (a) Spring deployment 4–17 April 2008. Black symbols mark location of Fairbanks (65°N) and Prudhoe Bay (70°N). (b) Summer deployment 29 June and 10 July 2008. Location of Cold Lake (54°N) shown with black diamond. Note seasonal scale change.

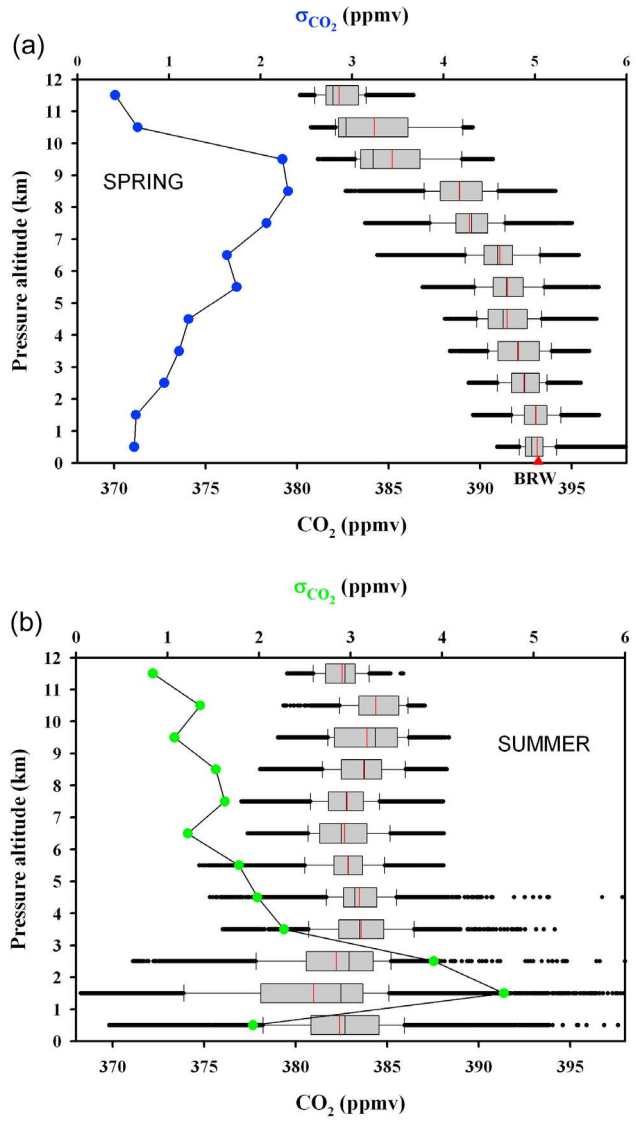

Figure 3. Statistical summary of observed CO_2 distributions. Vertical red line within each box represents the mean; black line is the median. Standard deviation of the mean for all vertical profiles inset. (a) Spring with mean CO_2 for Pt. Barrow indicated with a red triangle. (b) Summer.

intervals, reflecting the combined effect for all CO_2 sources and sinks. In the spring near-surface layer, the most evident latitudinal trend is the high CO_2 mixing ratios observed south of 70°N particularly over local urban/industrial sources located in Fairbanks, Alaska (65°N, 148°W) and Prudhoe Bay (70°N, 148°W). Most notable during spring are discrete plumes with enhanced CO_2 values in the mid-troposphere throughout the region surveyed. Above 8 km, the lowest CO_2 mixing ratios were associated with stratospherically influenced air masses (O_3 > 200 ppbv), and have a mean value of 382.7 ± 0.8 ppmv. During summer, greater variability is observed south of 60°N at all altitudes where maximum CO_2 mixing ratios were recorded over the continent below 1 km. A less frequent yet measurable stratospheric influence yielded a summer mean value of 383.1 ± 0.5 for altitudes ≥8 km indicating a seasonal difference of <0.5 ppmv in lower stratospheric air masses probed during ARCTAS. Differences in the ARCTAS sampling domains (Figure 1) are also reflected in these observations. In spring, measurements were made mainly over the Alaskan region; one of the major inflow regions of pollutants from Asia to the Arctic [*Fuelberg et al.*, 2010], while summertime observations were conducted further east.

[17] We can further explore these trends by summarizing the CO_2 data sets for both phases of ARCTAS using the box plots shown in Figure 3 that represent statistical values: 25th percentile (left box boundary); 75th percentile (right box boundary); and outliers (symbols) beyond the 95th and 5th percentiles (whiskers). These representations (Figure 3) clearly capture how dynamic this high northern latitude environment is by the pronounced seasonality exhibited by atmospheric CO_2. ARCTAS-A CO_2 distributions display a pattern of decreasing trend with height typically observed in spring with greater variability in the free troposphere than the lower atmosphere. Shown for reference is the mean (393.2 ± 0.7) in situ CO_2 surface data at Barrow, Alaska (BRW, 71°N, 157°W) over the duration of the spring local flights in comparison to the airborne observational mean (393.1 ± 1.0) for the 0–1 km layer (Figure 3a). In summer the magnitude of surface CO_2 exchange is large, reflected by the minima of CO_2 observed during ARCTAS-B. The pronounced variability below 3 km reveals active CO_2 sink processes juxtaposed alongside significant CO_2 sources. All the summer altitude bins contain CO_2 values below the measured spring minimum of 380 ppmv. In summarizing the overall statistics for both deployments: mean 390.8 ± 3.1 ppmv, median 391.5 ppmv, N = 204611, range 380.2–422.7 ppmv (ARCTAS-A); mean 382.8 ± 3.0 ppmv, median 383.1 ppmv, N = 177133, range 368.3–624.2 ppmv (ARCTAS-B) yielding a seasonal change between the two ARCTAS deployments of 8 ppmv (~2%) for daytime CO_2.

[18] The observed vertical distribution of CO_2 is an important indicator of the coupling between flux and transport processes influencing the CO_2 concentration field as much pollution transport takes place in the free troposphere [*Vay et al.*, 1999, 2003; *Choi et al.*, 2008] at heights typically unattainable by the surface monitoring network. Vertical profiling by aircraft aids the interpretation of surface observations by linking the surface with the boundary layer and free troposphere. During ARCTAS, the DC-8 executed seventy five vertical soundings from its nominal floor to ~12 km (~200 hPa). The standard deviation of the mean for all the aircraft profiles shows that in spring CO_2 exhibited the largest variability (<1%) in the mid-to-upper troposphere (6–10 km) (Figure 3a), while the variability was more pronounced (>1%) in summer yet occurred above the surface between 1 and 3 km (Figure 3b).

[19] Figure 4 illustrates the relationship of CO_2 and CO as a function of altitude observed during the two deployments. The overall correlation is significant for spring (Figure 4a), yet degraded by the influence of photosynthesis and respiration during the growing season (Figure 4b). In spring (Figure 4a), CO_2 and CO were highly correlated (slope = 0.073 ppmv $ppbv^{-1}$, r^2 = 0.97) above 8 km; the tight coupling likely attributable to a stratospheric influence evident from the decreasing CO_2 and CO concentrations with increasing altitude, as well as from remnants of an earlier seasonal cycle communicated from the surface to the upper troposphere over time.

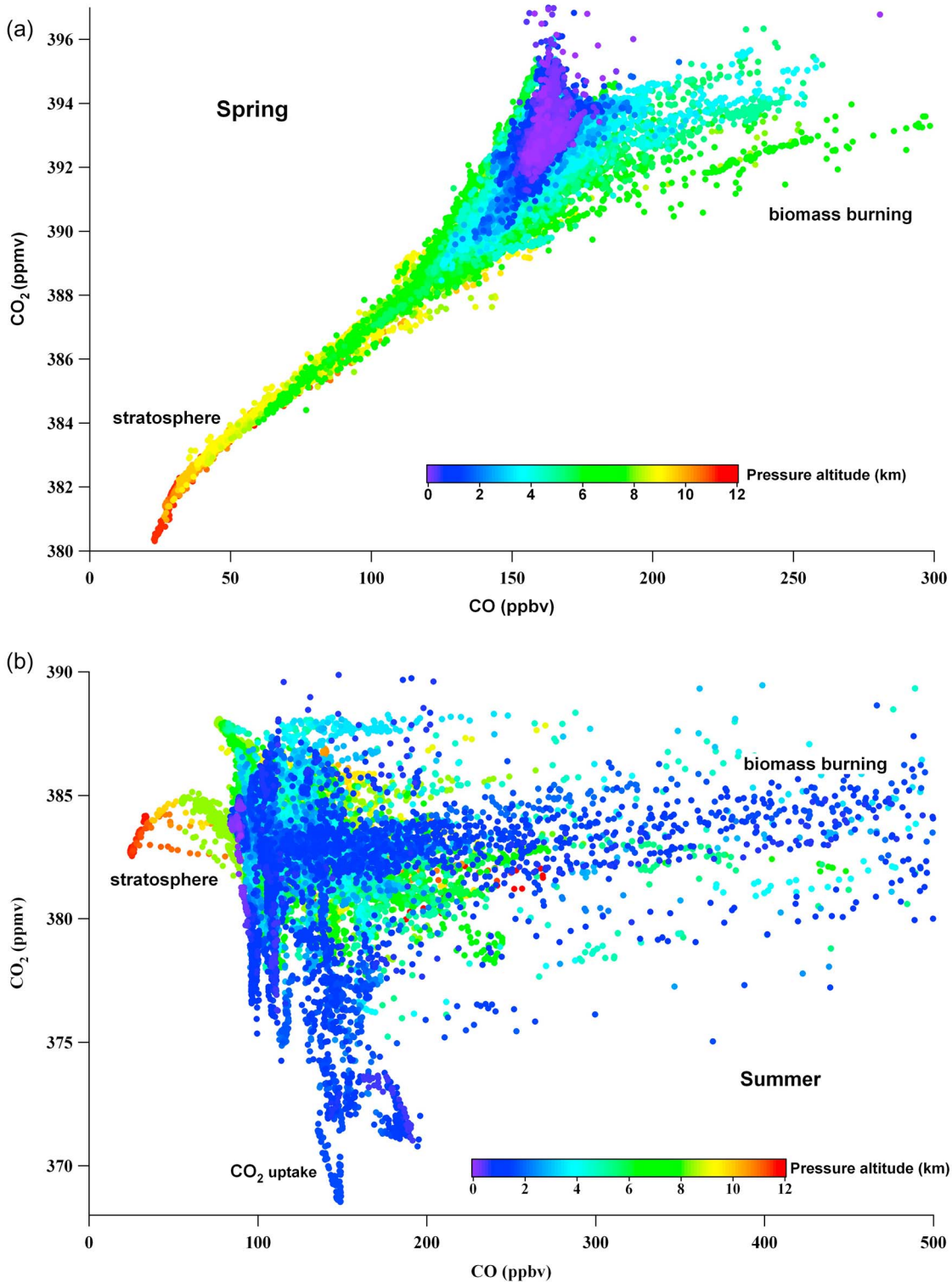

Figure 4. Regional correlations between CO_2 and CO. (a) Spring. (b) Summer.

[20] With diminishing height, this relationship begins to degrade revealing a multiplicity of sources influencing the ARCTAS-A sampling domain. A very different picture emerges in summer (Figure 4b) where the CO_2:CO correlation slopes reveal at least two distinct populations, and the reversal of source-sink relationships observed in spring.

4.2. ARCTAS-A Spring Deployment

[21] Although the spring DC-8 deployment focused on the long-range transport of anthropogenic pollutants to the Arctic, the influence from prominent smoke events linked to extensive fires in Russia and Kazakhstan was particularly evident [*Saha et al.*, 2010]. In 2008, the fire season in

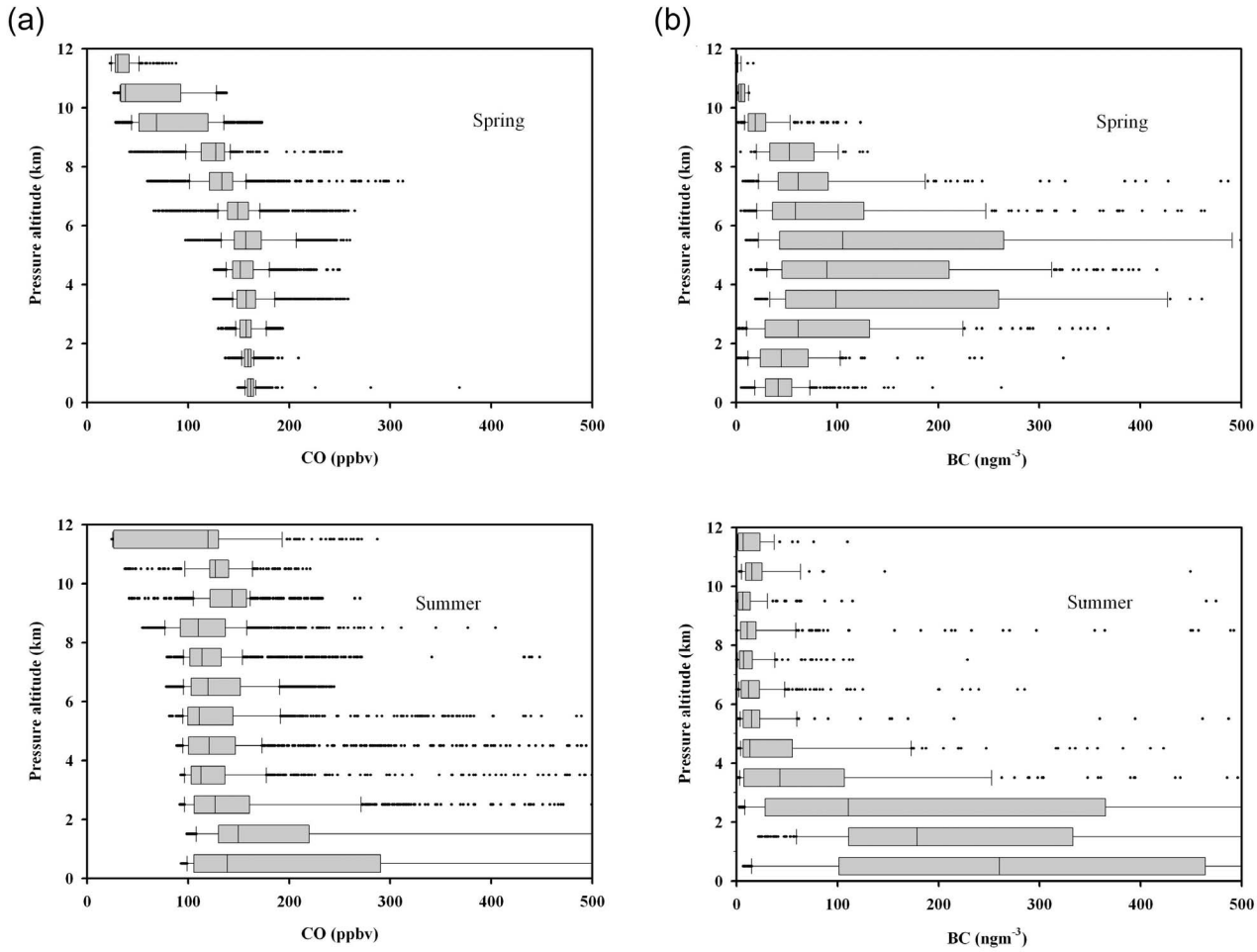

Figure 5. Statistical summary of the distributions observed in (top) spring and (bottom) summer for (a) CO, (b) BC, (c) CH_3CN, and (d)C_2Cl_4.

Russia began unusually early due to low snow cover that year [*Warneke et al.*, 2009]. Colder air temperatures in early spring facilitated the transport of forest and agricultural fire emissions into the Arctic from the southern Siberia–Lake Baikal area and Kazakhstan–southern Russia, respectively with a typical transport time of 4–9 days [*Fuelberg et al.*, 2010].

[22] The perturbation of the Arctic and sub-Arctic atmosphere by episodes of pollution is apparent in the source tracer plots presented in Figure 5 that reflect clean (25th percentile), median, and polluted conditions (≥75th percentile). CO, BC, CH_3CN, and C_2Cl_4 are enhanced and, similar to CO_2, are more variable above 3 km indicating a mixture of anthropogenic and fire emissions having a strong imprint on atmospheric concentrations. Using CO observations from the ARCTAS-A and ARCPAC airborne campaigns as top-down constraints in the chemical transport model GEOS-Chem, *Fisher et al.* [2010] attributed this free-tropospheric variability predominately to Asian anthropogenic emissions; and Russian biomass burning (BB), which contributed substantially to CO variability in the form of combustion plumes. In investigating the distribution of BC, *Matsui et al.* [2011] found that most Asian anthropogenic air parcels were transported from lower latitudes (30°N–40°N), experiencing rapid ascent by WCBs and were generally measured in the Arctic upper troposphere. The Russian BB air parcels however, originated from higher latitudes (50°N–70°N) and arrived in the Arctic middle troposphere following near isentropic slow ascent [*Matsui et al.*, 2011].

[23] We examined data from three of the DC-8 flights (4/12, 4/16, 4/17) conducted over the Alaskan Arctic/sub-Arctic for evidence of biomass burning plumes (Figure 1a). Stratospheric air influences were first removed from the data set using the filter $[O_3]/[CO] > 1.25$ mol mol^{-1} [*Hudman et al.*, 2007]. Fire plumes were then identified as having CO in excess of 160 ppbv, the median observed CO concentration at the surface (Figure 5a); and CH_3CN values >225 pptv, an unambiguous enhancement in CH_3CN mixing ratios (Figure 5c). Where CH_3CN data were unavailable, HCN mixing ratios >500 pptv were used (not shown). From thirty smoke plumes intercepted between 3.5 and 7.5 km, we determined a mean CO_2 to CO enhancement ratio of 54 ± 18 ppmv ppmv^{-1}. The slopes ranged from 27 to 83 ppmv of CO_2 per ppmv of CO, the values reflecting the transport of emissions under varying meteorological conditions from influential source regions having different fuel types, fire temperatures, and combustion phases (flaming, smoldering, mixed); as well as the mixing of plumes from different source

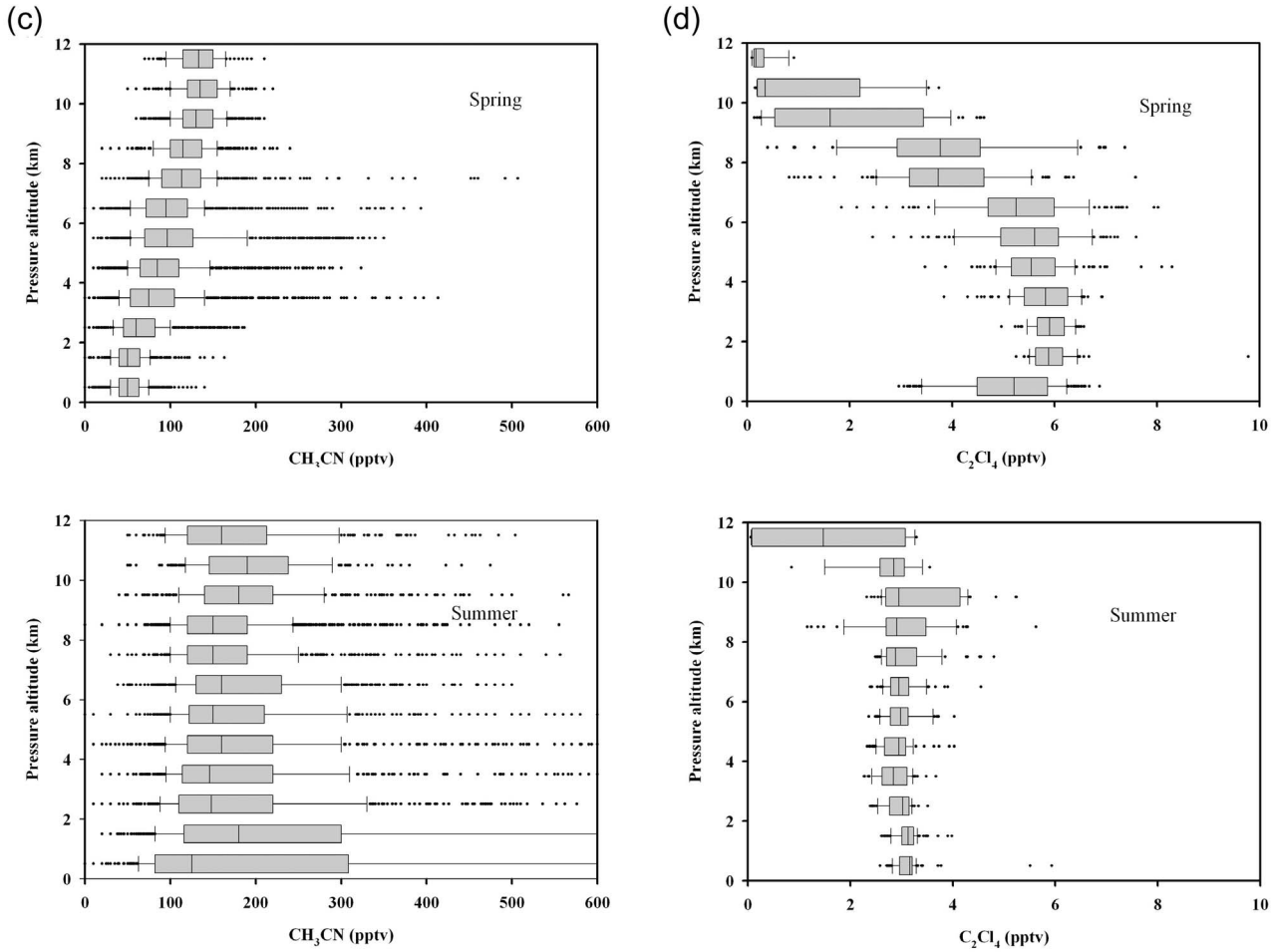

Figure 5. (continued)

regions, and distance of sample collection relative to the fires (A. Hecobian et al., Comparison of the chemical and physical evolution and characteristics of 495 biomass burning plumes intercepted by the NASA DC-8 Aircraft during the ARCTAS/CARB-2008 field campaign, submitted to *Atmospheric Chemistry and Physics Discussions*, 2011).

[24] To explore anthropogenic contributions to the fire plumes and compare ARCTAS-A and ARCPAC results, we subdivided our plume data set based on sampling height: ≤6.5 km (highest flight level of the NOAA WP-3D aircraft) and ≥6.5 km. As reported by *Warneke et al.* [2009], only small enhancements in C_2Cl_4 were observed in the fire emissions probed by the NOAA WP-3D (C_2Cl_4:CO ~ 0.002 pptv $ppbv^{-1}$), indicating a nearly negligible contribution from anthropogenic pollution to the plumes. The ARCTAS-A plume subset for ≤6.5 km (n = 21) yielded a similar result (C_2Cl_4:CO ~ 0.004 pptv $ppbv^{-1}$). The mean enhancement ratio of C_2Cl_4 was significantly higher (0.0212 pptv $ppbv^{-1}$) though for DC-8-based sampling in plumes above 6.5 km (n = 9), substantiating a mixture of industrial/urban/fire emissions influencing the composition of the Arctic upper atmosphere. This value is consistent with midtropospheric C_2Cl_4:CO observations by *de Gouw et al.* [2004] in polluted air masses transported from Asia to the U.S. west coast. From Figure 1a showing the plume locations, it is evident that the spatial extent of the pollution extended far beyond North American continental margins, penetrating the high Arctic. Of the nine plumes examined containing a mixture of anthropogenic and BB emissions, 78% were intercepted by the DC-8 poleward of 80°N. Figure 6a captures one of these high northern latitude pollution events encountered on 17 April, apparent from the several sharply defined plumes enriched in CO_2, CO, C_2Cl_4, BC, and CH_3CN.

[25] In addition to determining the CO_2:CO enhancement ratios for the nine plumes (Table 2), we investigated their respective chemical signatures and transport pathways to tag anthropogenic emission source regions. To illustrate the approach used, two of the plumes intercepted by the DC-8 are presented here in detail. We initially examine plume 1 sampled at 85°N, 150°W (Figure 1a), having a CO_2:CO enhancement ratio of 27 ppmv $ppmv^{-1}$ (Table 2). Using the Lagrangian particle dispersion model, FLEXPART [*Stohl et al.*, 2002] (http://transport.nilu.no/flexpart-projects?cmp = ARCTAS), with meteorological input from the National Center for Environmental Prediction (NCEP) Global Forecast System (GFS) model, the FLEXPART emissions sensitivity footprint (Figure 7a) reveals that the sampled air mass traveled over Siberia, continuing eastward

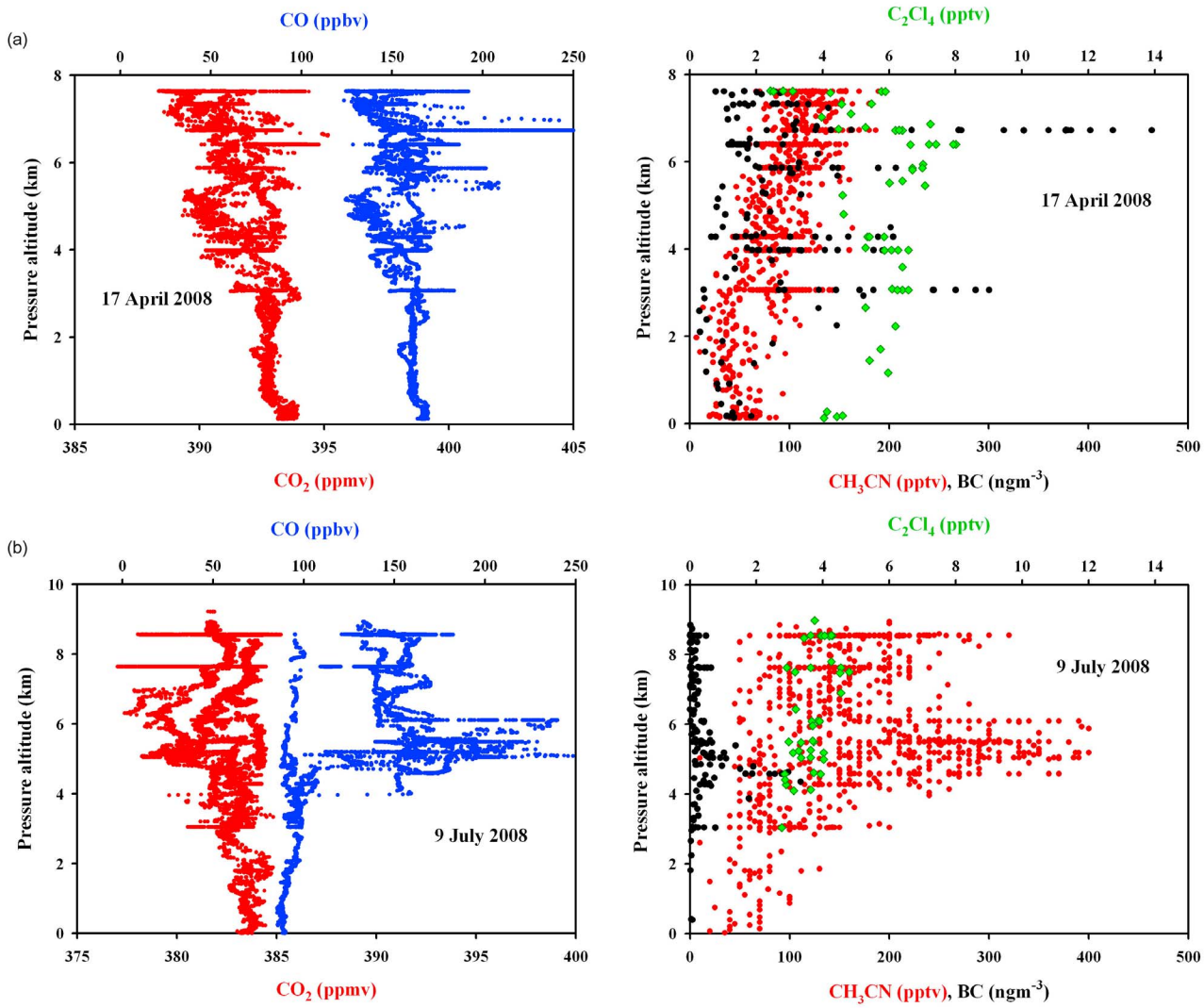

Figure 6. Selected plume composition for pollution events sampled poleward of 80°N. (a) Spring. (b) Summer.

over China and North America prior to reaching the North Pole. The air parcel was in contact with the atmospheric boundary layer (ABL) 8–11 days prior while over Siberia and Northeastern China (Figure 7a), facilitating the surface uptake of fire and urban/industrial emissions en route as reflected in the CO_2 (394 ppmv), CO (314 ppbv), C_2Cl_4 (7.5 pptv), and HCN (738 pptv) enhancements. The correspondingly low CO_2:CO likely results from inefficient combustion processes relating to the fires and/or domestic combustion sources (e.g., coal, biofuel). Given conservation

Table 2. Measured and Estimated Statistics for Anthropogenic Plumes[a]

Anthropogenic Plume	Latitude (°N)	Longitude (°W)	Maximum CO_2 (ppm)	Maximum CO (ppb)	CO_2:CO (ppm:ppm)	R^2	Source Region	Initial ABL Contact (days)
1	84.725	−149.901	393.9	313.7	26.9	0.86	Asian	6
2	86.715	−154.453	393.3	267.8	29.7	0.95	Asian	5
3	81.709	−142.248	393.1	201.7	47.2	0.86	Eurasia	10
4	65.073	−147.692	393.9	235.0	45.1	0.92	Eurasia	3
5	89.381	−148.447	394.8	187.0	80.4	0.88	Europe	4
6	84.278	−156.769	391.9	163.3	76.4	0.93	Europe	11
7	80.012	−156.332	394.4	192.1	80.1	0.71	Europe	4
8	75.849	−155.982	390.9	183.8	36.5	0.70	NA	5
9	81.495	−156.520	394.0	208.7	52.1	0.93	NA	10–11

[a]Air parcel classification and time since emissions uptake.

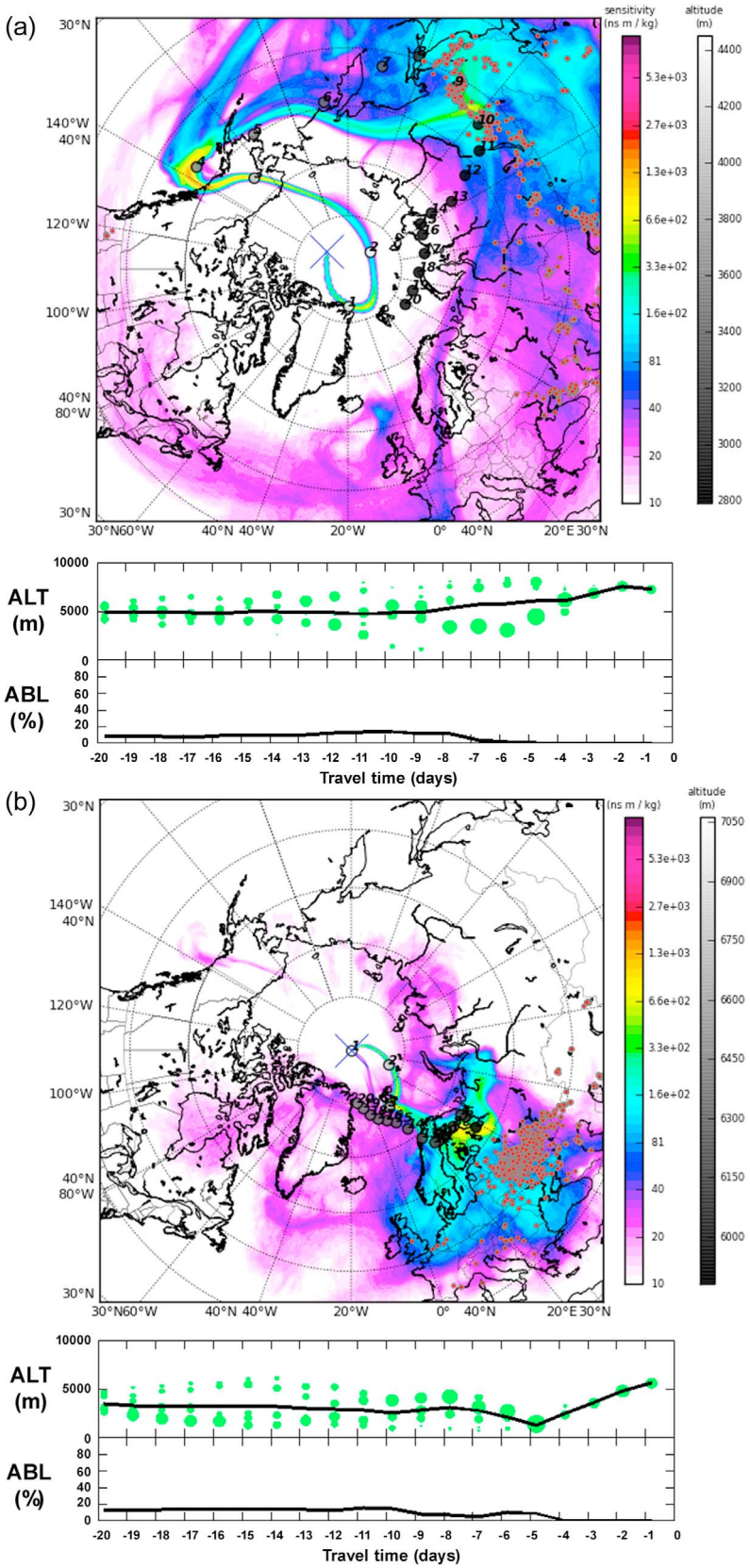

Figure 7. FLEXPART emission sensitivity footprints illustrating transport history of pollution sampled north of 80°N. Numbers represent travel time of the air parcel in days, while red circles depict MODIS active fire counts (a) for plume 1 and (b) for plume 5.

Table 3. Atmospheric Lifetime, Background Averages, and Measurement Statistics for Selected Compounds in the Anthropogenic Plumes

Compound	Formula	Lifetime	Background Average (pptv)	Enhancement Over Average Background (%)			
				Asia	Europe	North America	Eurasia
Tetrachloroethene	C_2Cl_4	2–3 months	4.2	65.2	42.8	14.9	47.9
1,2-Dichloroethane	$C_2H_4Cl_2$	1–2 months	11.0	76.8	20.9	25.5	40.0
Carbonyl Sulfide	OCS	2.5 years	487.0	35.7	1.7	8.9	1.0
Ethyl chloride	C_2H_5Cl	30 days	2.5	65.4	25.8	7.8	43.4
Propane	C_3H_8	11 days	312.0	78.8	90.7	26.9	84.8
Methyl chloride	CH_3Cl	1 year	567.0	14.5	4.2	8.2	4.4
Benzene	C_6H_6	9 days	49	273.5	151.5	80.6	225.5

of the tracers during transport, the ratio is representative of winter 2007 values reported by *Wang et al.* [2010] for Central Eastern Siberia (33.1 ppmv $ppmv^{-1}$) and Northern China (28.6 ppmv $ppmv^{-1}$). In contrast, an 80 ppmv $ppmv^{-1}$ slope was associated with plume 5 (89°N, 148°W) (Figure 1a) enhanced in CO_2 (395 ppmv) and C_2Cl_4 (8 pptv), yet with comparatively lower CO (187), and HCN (627 pptv); a more pronounced urban/industrial signature. Inspection of a combination of FLEXPART products (Figure 7b) indicates emissions uptake 4 days earlier over Northeastern Europe with rapid transport from northern Europe directly to the pole. This CO_2:CO correlation slope is within the range of emission ratios (64.5–82.6 ppmv $ppmv^{-1}$) determined from surface-based measurements made within the European continent [*Vogel et al.*, 2010; *Gamnitzer et al.*, 2006]. It is also comparable to that sampled in the outflow from Japan (80 ppmv $ppmv^{-1}$) [*Suntharalingam et al.*, 2004], a country with cleaner combustion technologies [*de Gouw et al.*, 2004], suggesting a higher combustion efficiency for the indicated source region.

[26] Attributes of the other plumes were similarly investigated, arriving at the source region classification presented in Table 2 that exhibits relatively tight clustering in enhancement ratio values. The background average for each chemical tracer used (Table 3) was determined by first removing any stratospheric influence from the ARCTAS-A observations, then calculating the lowest quartile (25%) of the remaining data [*Harrigan et al.*, 2011]. Summarizing from Table 3, all of the plumes were enriched in C_6H_6, indicating uptake of anthropogenic emissions ≤9 days prior to measurement. Mean C_2Cl_4 values in the plumes were enhanced 20–80% over background. The suite of tracers used for chemically fingerprinting Chinese/Asian air masses, 1,2-DCE, OCS, CH_3Cl, and ethyl chloride [*Barletta et al.*, 2009], exhibited significantly elevated mixing ratios within the two plumes comprising the Asian category; further supporting their initial source region classification using FLEXPART. Furthermore, large enhancements in propane absent a corresponding increase in methane (not shown) likely reflect a greater reliance upon liquefied petroleum gas (LPG) in three of the four source region categories.

4.3. ARCTAS-B Summer Deployment

[27] Of the 1.5 million hectares (Mha) that burned in Canada in 2008, 73% were consumed by fires in Saskatchewan, with 0.75 Mha burning in the remote northern regions of that province. The Saskatchewan burned area significantly exceeded the 20 year mean while overall Canadian fires were near normal [*Soja et al.*, 2008]. Many of these forest fires were allowed to burn naturally, thus tending to be larger than those in regions where fires were actively suppressed, and typically developed smoke columns reaching 5–7 km. The distributions of CO, BC, CH_3CN, and C_2Cl_4 during the summer deployment (Figure 5) reflect a seasonal shift in the pollution influence from the middle to the lower troposphere. The perturbation from biomass burning on atmospheric composition is apparent in the large enhancements in CH_3CN absent elevated C_2Cl_4 mixing ratios (Figure 5) revealing fire emissions significantly influencing the summer sampling domain.

[28] Three of the ARCTAS-B flights (6/29, 7/01, 7/04) (Figure 1b) extensively sampled sub-Arctic central Canadian wildfire emissions over areas far removed from large urban complexes. In Figure 8, remote sensing data products from the SPOT and MODIS sensors capture the vegetation types and fire activity within this region during the DC-8 overflights. Land cover types are from the GLC-2000 database generated from daily 1 km data [*Fritz et al.*, 2003] acquired by the VEGETATION instrument onboard the SPOT 4 satellite. The MODIS active fires represent the diurnal fire cycle when both the Terra and Aqua satellites were simultaneously collecting data [*Giglio et al.*, 2006]. The MODIS data are at 1 km spatial resolution but under ideal conditions, flaming combustion can be detected at 50 m^2. This image indicates the majority of measurements were over fires consuming a stand composition predominately comprised of evergreen needleleaf forests.

[29] Figure 9 shows the airborne CO_2 data for the three flights over the region bounded by 50°N–60°N, 80°W–120°W. Also plotted for reference are in situ CO_2 observations from the Canadian surface monitoring stations East Trout Lake (ETL), Saskatchewan (54.35°N, 104.98°W); Lac Labiche (LLB), Alberta (54.95°N, 112.45°W); and Fraserdale (FSD), Ontario (49.84°N, 81.52°W) [*Worthy et al.*, 2009; *Higuchi et al.*, 2003]. For each surface station, in situ CO_2 measurements were averaged over the interval of 15:00–17:00 (local time); a period of quasi-constant CO_2 mixing ratio [*Higuchi et al.*, 2003] coinciding with each of the three afternoon DC-8 sampling sorties, planned to capture peak fire activity. In Figure 9, CO_2 enriched fire plumes are evident, particularly those sampled below 2 km, west of 100°. The highest mixing ratios of CO_2 (624 ppmv) and CO (14 ppmv) observed during ARCTAS (1 July, 56°N, 107°W, 0.9 km) were measured in these boreal wildfire emissions. Eastward out of the fire influence, lower CO_2 mixing ratios in the airborne observations reflect uptake by the terrestrial biosphere undisturbed by fire. Undoubtedly, some of the summertime CO_2 observations reflect a mixture

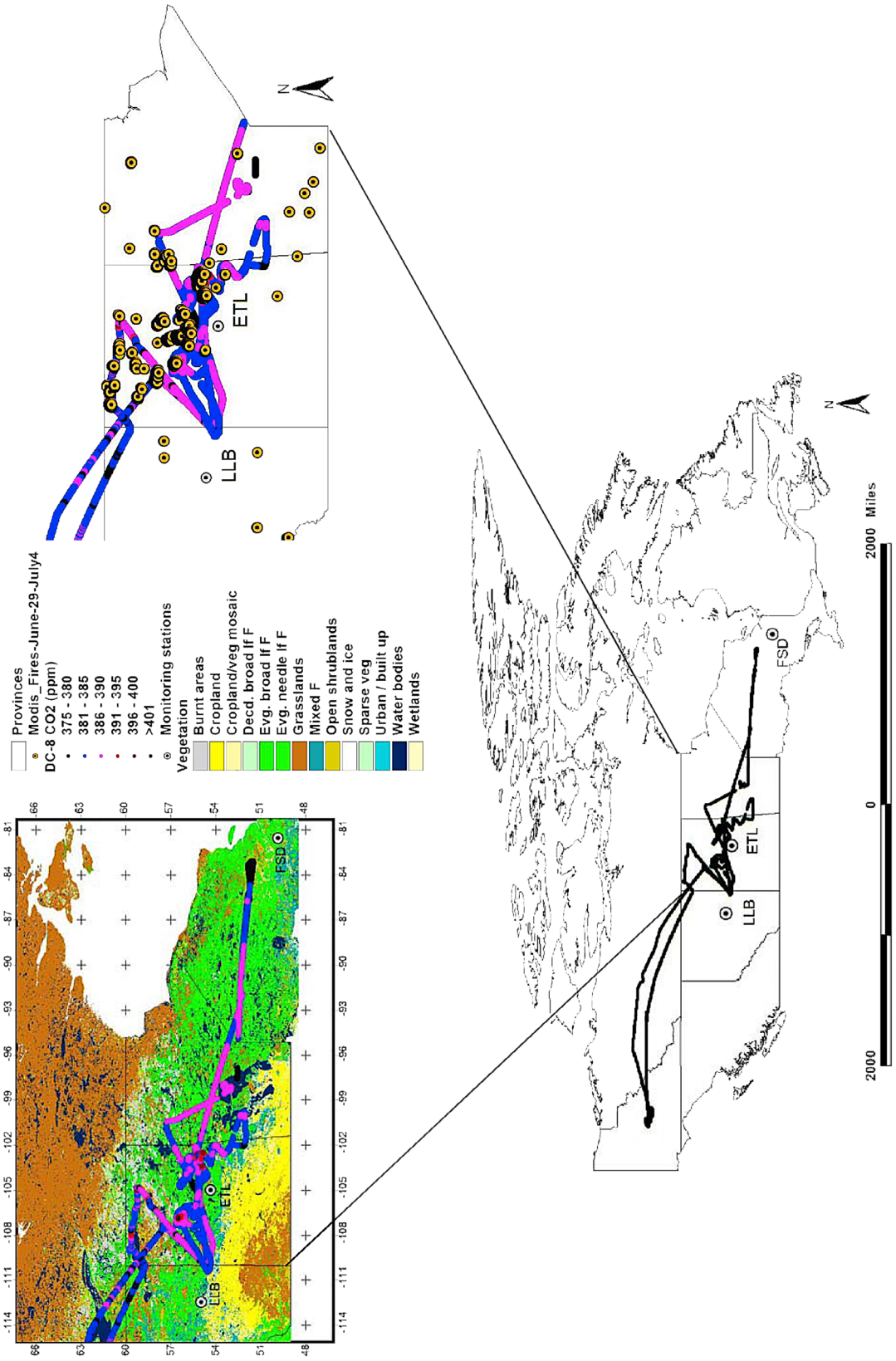

Figure 8. Vegetation classification based on the Envisat SPOT sensor overlain with CO_2 distributions along DC-8 flight tracks (top left). Yellow symbols represent active fires detected by the MODIS sensor relative to the CO_2 measurements (top right).

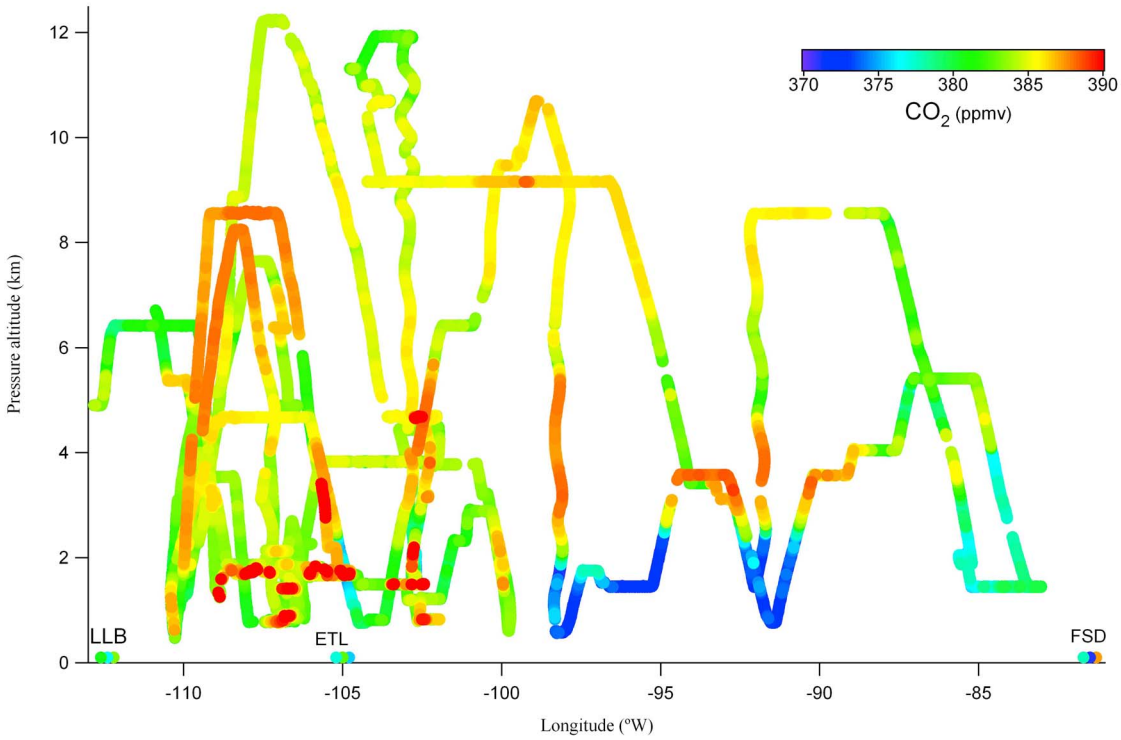

Figure 9. CO_2 concentrations over wildfires in Saskatchewan Province measured between 50°N and 60°N, 80°W and 120°W, 29 June to 4 July 2008. CO_2 data from Environment Canada's East Trout Lake (ETL), Lac Labiche (LLB), and Fraserdale (SD) surface monitoring sites are shown for reference. Surface data are averaged over the afternoon interval of 15:00–17:00 local time for each flight day.

of fire (source) and biospheric uptake (sink) signals that tend to compensate one another; a complication for quantification of the two individual terms since CO_2 mixing ratios from the combined fluxes can exhibit a low deviation from background CO_2 levels.

[30] From the 39 identifiable smoke plumes resulting from active boreal wildfires, we find a mean CO_2:CO emission ratio of 8.9 ± 3.5 ppmv ppmv^{-1} in direct fire emissions sampled ≤2 km. The CO_2:CO slopes ranged from 4 to 16 ppmv ppmv^{-1} and there was a negligible contribution to the plumes from anthropogenic sources based on the C_2Cl_4 data.

[31] We can calculate an approximate emission factor for CO_2 using an equation given by *Alvarado et al.* [2010]:

$$EF_{CO2} = M_{CO2} \cdot ER_{CO2} \cdot (1 - MCE) \cdot f_C / M_C$$

where EF_{CO2} is the emission factor in g kg^{-1} dry matter (DM) burned, M_{CO2} is the molecular weight (g/mol), ER_{CO2} is the emission ratio of CO_2 to CO (mol/mol), M_C is the molecular weight of carbon (0.012 kg C/mol), and f_C is the mass fraction of carbon in the biomass. In general, it is assumed that all the volatilized carbon is detected and that the fuel is 50% carbon by mass [*Susott et al.*, 1996; *Goode et al.*, 2000] thus we use an f_C value of 0.5 kg C/kg dry matter for this analysis. Modified combustion efficiency (MCE = $1/((\Delta CO/\Delta CO_2) + 1)$) [*Ward and Radke*, 1993; *Yokelson et al.*, 1996; *Goode et al.*, 2000], a unitless indicator of the fire's combustion phase during sampling, varies from approximately 80% to near 99% for purely smoldering and flaming combustion, respectively. Values above 90% suggest a ≥50% contribution from flaming combustion. MCE values from our observations spanned 0.83–0.95. The mean EF for CO_2 in examined wildfire plumes was 1698 ± 280 g kg^{-1} DM, with a median value of 1634 g kg^{-1} DM; consistent with previously reported values from empirical studies investigating boreal fire emissions [*Hegg et al.*, 1990; *Goode et al.*, 2000; *Akagi et al.*, 2011; *Simpson et al.*, 2011].

[32] As in spring, pollution continued to penetrate the high Arctic during summer. During the 9 July flight, the mid-to-upper tropospheric CO and CH_3CN data (Figure 6b) expose a fire fingerprint that is likely embedded and thus obscured in the CO_2 biospheric uptake signal that dominates in summer. *Fuelberg et al.* [2010] note that fires over Asia continued in summer and were more widespread than in spring; with the majority of these fires located near and west of Beijing, emitting plumes at times reaching the North Pole. The broad peak in the altitude distributions of CO and CH_3CN indicate a dominate influence from BB in the middle troposphere. Markedly lower C_2Cl_4 mixing ratios reveal a smaller contribution from anthropogenic sources than in spring, while the BC data reflect wet removal processes during transport mainly due to the higher precipitation rates in summer [*Matsui et al.*, 2011]. Pollution reduction strategies in effect in Beijing for the 2008 summer Olympics [*Witte et al.*, 2009] may, in part, be reflected in the observed lower urban/industrial signal. The scatter is too great in the CO_2:CO relationships of these aged plumes to provide meaningful information. In summer, the magnitude of CO_2

Table 4. Characteristics of $^{14}CO_2$ Station Records

Surface Site	Location, Elevation (masl)	Station Classification	Monthly Mean ± sd	
			April 2008	July 2008
Niwot Ridge (NWR)	40°N, 105°W, 3523	U.S. Continental	46.4 ± 0.1‰ (n = 5)	47.7 ± 0.4‰ (n = 5)
Jungfraujoch (JFJ)	46°N, 8°E, 3450	European Continental	46.2 ± 2‰ (n = 2)	49.1 ± 2‰ (n = 2)
Pt. Barrow (BRW)	71°N, 157°W, 11	Arctic	43.2 ± 0.3‰ (n = 2)	47.5 ± 2.8‰ (n = 4)

variance driven by surface exchange with soils and vegetation exceeds the variance from combustion sources, hence CO_2:CO correlations are low [*Wang et al.*, 2010].

5. Radiocarbon

[33] Measurements of $\Delta^{14}C$ in atmospheric CO_2 ($\Delta^{14}CO_2$) can be an effective method of parsing biogenic and fossil fuel contributions to the total measured CO_2 signal. Fossil fuel derived CO_2 is entirely devoid of the rare radioactive isotope ^{14}C, due to its extreme age; isotopes ^{12}C and ^{13}C remain in CO_2 produced from the combustion of fossil carbon. The addition of ^{14}C-free fossil fuel CO_2 to the atmosphere increasingly dilutes the $^{14}CO_2/^{12}CO_2$ ratio, thus lowering the atmosphere's ^{14}C content [*Suess*, 1955]. These ratios, reported as $\Delta^{14}CO_2$, can be precisely quantified in atmospheric samples. Emissions from fossil fuel combustion add CO_2 with a $\Delta^{14}C$ of −1000‰, thus a $^{14}C/^{12}C$ ratio lower than the clean air level indicates the influence of fossil fuel combustion CO_2 sources in the sampling environment [*Levin et al.*, 1980; *Turnbull et al.*, 2006; *Hsueh et al.*, 2007; *Graven et al.*, 2009].

[34] Local biological activity is usually considered to be an important contributor to the mass balance of CO_2 [*Newman et al.*, 2008; *Naegler and Levin*, 2009], particularly during the growing season when biogenic respiration is high due to increased metabolic activity. The biospheric release of ^{14}C-enriched CO_2 during heterotrophic respiration alters $\Delta^{14}C$ in local CO_2, leading to a positive $\Delta^{14}CO_2$ disequilibrium [*Randerson et al.*, 2002; *Hsueh et al.*, 2007; *Turnbull et al.*, 2009] (i.e., biosphere-atmosphere) that is not well known and may be quite heterogeneous over different species and ecosystems [*Graven et al.*, 2009]. A disequilibrium estimate on the order of 15–40‰ was recently reported by *Naegler and Levin* [2009] for the year 2005. CO_2 emissions from biomass burning may have a much larger positive $\Delta^{14}CO_2$ disequilibrium than heterotrophic respiration, due to the longer residence time of carbon in forests [*Turnbull et al.*, 2009] and residual sources from aboveground nuclear weapons testing in the late 1950s and early 1960s [*Djuricin et al.*, 2010]. Biomass burning constitutes an additional source either unaccounted for in the mass balance approach or one that is often rolled into the respiration term because the fire CO_2 flux has been quite small. In recent years, however, unprecedented fire activity has occurred in boreal ecosystems, notably in 2003, 2004, 2008, and 2010. Fire within these ecosystems can accelerate the release of carbon assimilated years ago, sending pulses of enriched $\Delta^{14}CO_2$ into the atmosphere. The contribution to atmospheric CO_2 from this temporally varying perturbation is likely attributed to biogenic respiration since $\Delta^{14}CO_2$ cannot be used to distinguish between fire-induced combustion of biomass and heterotrophic respiration [*Djuricin et al.*, 2010] without an accompanying fire specific tracer. Moreover, resulting high excursions in $\Delta^{14}CO_2$ may be ascribed to a stratospheric influence, cosmogenic production, a nuclear power source, or excluded from an analysis.

[35] *Levin et al.* [2010] point to serious gaps in our understanding of the mechanisms controlling the interannual and seasonal $\Delta^{14}CO_2$ variability. They conclude that the $\Delta^{14}CO_2$ seasonality today is dominated by respective temporal atmospheric transport patterns, which exert a seasonal signal on $\Delta^{14}CO_2$ mainly because of the large spatial gradients caused by fossil fuel combustion. Since long-range transport processes are often decoupled from the surface, airborne observations of $\Delta^{14}CO_2$ offer unique insight into the vertical propagation and mixing of particular sources of CO_2 [*Vay et al.*, 2009; *Graven et al.*, 2009]. Below, we present results from investigating fossil fuel, biogenic, and biomass burning contributions to ARCTAS CO_2 observations using the combination of isotopic $\Delta^{14}CO_2$, fire and other chemical tracers along with transport histories to gain further insight into these processes.

[36] The $\Delta^{14}C$ level in atmospheric CO_2 was determined from air remaining in a select subset of whole air canister samples (n = 48) collected onboard the DC-8 for measurements of hydrocarbons and halocarbons [*Simpson et al.*, 2010, 2011]. Grab samples were acquired preferentially in pollution layers in contrast to the continuous measurements of CO_2. Our objective was to quantify any fossil fuel component of the total measured in situ CO_2 signal, and to investigate influences on the observed short-term or synoptic scale variability of $\Delta^{14}CO_2$ from the subset of whole air samples extracted for radiocarbon analysis.

[37] The background composition (Δ_{bg}) for this analysis is based on the high-precision atmospheric $\Delta^{14}CO_2$ records from the clean-air (background) stations listed in Table 4. Data from Alert (82°N, 62°W) were unavailable for inclusion in this study. From Table 4, monthly mean values reveal a small meridional gradient in tropospheric $\Delta^{14}CO_2$ during the spring ARCTAS deployment, on the order of 3‰, while there is no latitudinal trend evident in the summer data. As mentioned earlier, much of the pollution observed in the free troposphere was transported to the study region from significantly different emissions source regions and latitudes. Since transport from different latitudes might affect the choice of a reference background value of $\Delta^{14}CO_2$, we use the range of monthly mean values from the stations located between 40°N and 70°N in our analysis. Coupling the monthly mean values with the measurement precision (±2‰) indicates a range for the April $\Delta^{14}CO_2$ background of 41.2–48.4‰, and 45.5–51.1‰ for July. We note this yields latitudinal gradients of 7.2‰ and 5.6‰, respectively; larger than the few per mil reported [*Levin et al.*, 2010], thus leading to conservative estimates from our analysis. For spring $\Delta^{14}CO_2$ samples collected in the BL having a local influence, only the BRW data are

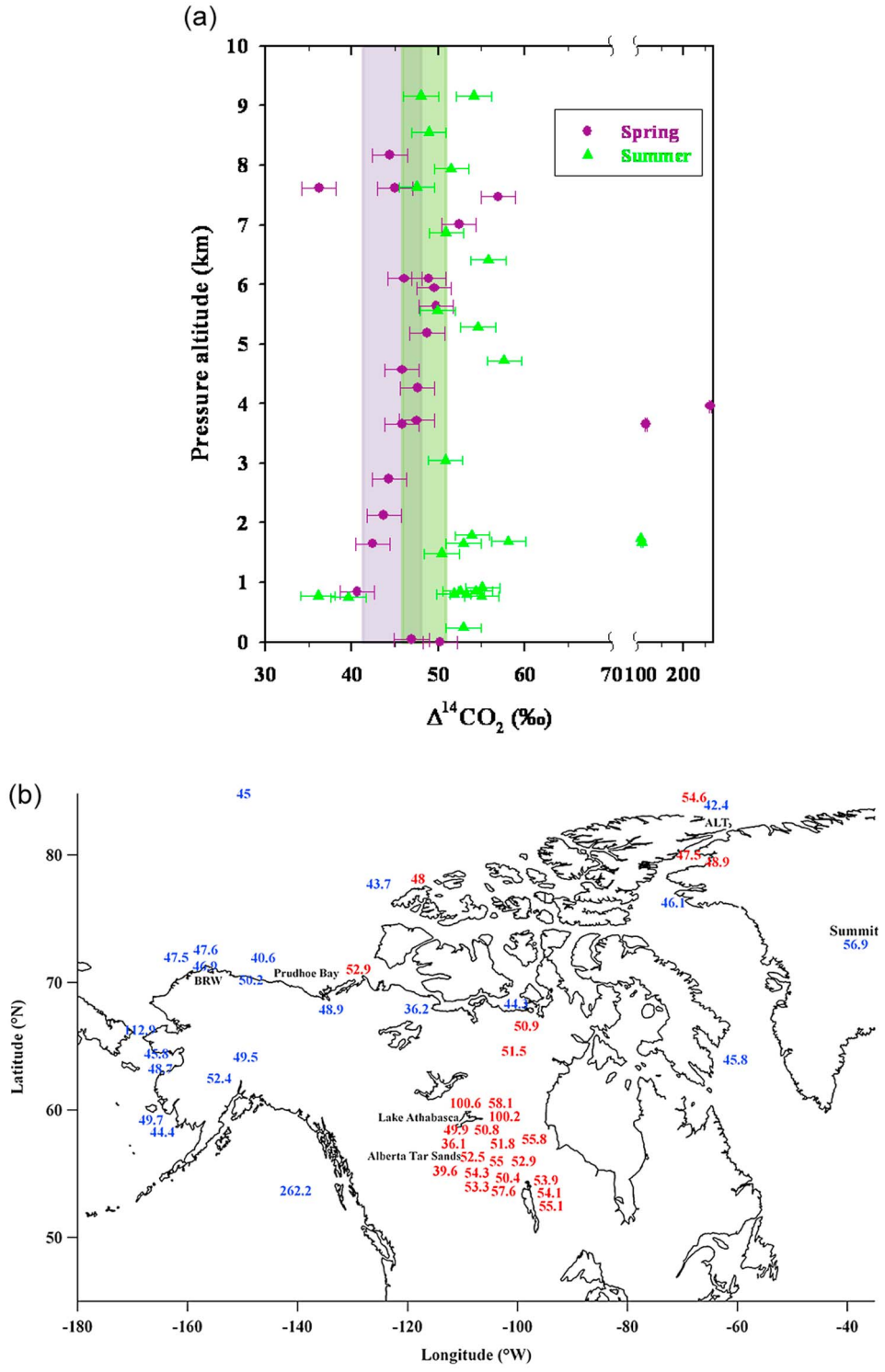

Figure 10. (a) Vertical distribution of $\Delta^{14}CO_2$. Shaded regions reflect the latitudinal range of spring and summer background $\Delta^{14}CO_2$ values from clean air monitoring sites. (b) Spatial pattern of $\Delta^{14}CO_2$ distributions: blue text for spring samples and red text for summer samples.

used as a clean air reference. Since there is no clean air station in close proximity to where the fresh fire emissions were sampled in summer, we use the July range of background values.

[38] The results from the ARCTAS airborne $\Delta^{14}CO_2$ observations are presented in Figure 10a, the shaded regions depicting respective temporal background windows as described above. Overall, spring measurements ($\leq 2\sigma$) had

an average $\Delta^{14}CO_2$ value of 46.6 ± 4.4‰ (n = 20), while the summer average was 51.5 ± 5‰ (n = 24) revealing a seasonal difference of approximately 5‰. ARCTAS sampling preceded both the May minimum and September maximum $\Delta^{14}CO_2$ periods reported by *Xu et al.* [2004] for BRW where the seasonal amplitude is typically 10‰.

[39] During sampling times, $\Delta^{14}CO_2$ values indicate fossil fuel combustion was not a dominant source of CO_2 (Figure 10a). Rather ARCTAS $\Delta^{14}CO_2$ observations revealed predominately a pattern of positive disequilibrium with respect to background ($\Delta_{veg} > \Delta_{bg}$) regardless of season. In the April data set, only two measurements were depleted in $\Delta^{14}CO_2$. One sample (40.6‰) was collected at 0.8 km in the vicinity of the Prudhoe Bay oil and gas processing facilities (Figure 10b) in an air mass with recent BL contact (<2 days prior), and contained elevated C_2Cl_4 (6.2 pptv) and i-pentane (50 pptv). Anthropogenic emissions in China (30°N–40°N) were accessed for transport to the Arctic resulting in the second depleted $\Delta^{14}CO_2$ value (36.2‰). This sample was collected at 7.6 km, and contained enhanced 1,2-DCE (53%), OCS (6%), CH_3Cl (9%), and ethyl chloride (89%); the suite of tracers used for chemically fingerprinting Chinese/Asian air masses [*Barletta et al.*, 2009].

[40] Eight samples (36%) collected within the free troposphere between 3.5 and 8 km were enriched in $\Delta^{14}CO_2$. The source of $\Delta^{14}CO_2$ enrichment in three of these samples (48.9, 49.7, 56.9‰) was likely the biospheric release of ^{14}C-enriched CO_2 during respiration as fire tracers are not elevated and concurrent O_3 measurements do not support a stratospheric influence. A $\Delta^{14}CO_2$ content of 56.9‰ was registered within an air mass sampled over Summit that originated from the subtropical North Atlantic (not shown). This air parcel was unique among the eight sampled, containing low CO_2 (388.8 ppmv), CO (125 ppbv), and C_2Cl_4 (3.7 pptv). CH_3CN (≤519 pptv) and/or HCN (≤1.3 ppbv) were enhanced in the five remaining enriched samples (48.7, 49.5, 52.4, 112.9, 262.2‰), with Siberian and Kazakhstan emission source regions indicated. For $\Delta^{14}CO_2$ samples within 2σ of the upper clean air value (48.4‰), we find a minimum disequilibrium of 0.3 to 4‰ likely due to biomass combustion and/or biospheric respiration.

[41] Four additional samples (44.3, 43.7, 46.9, 50.2‰) were collected within the BL in proximity to BRW and Prudhoe Bay (Figure 10b); their content and FLEXPART (not shown) reflecting local emission sources. One of the samples was captured during a missed approach by the DC-8 over Barrow at 0.04 km on 9 April, and exhibited a slight enrichment (46.9‰) compared to the BRW surface observations (43.2‰). Despite enhancements in the combustion tracers, C_2Cl_4, i-pentane (≤176 pptv), and propane (≤1224 pptv), the $\Delta^{14}CO_2$ values did not reflect a fossil fuel CO_2 influence. Absent elevated fire tracers, the enrichment observed is attributed to biospheric respiration.

[42] Two high $\Delta^{14}C$ excursions (112.9, 262.2‰) were tagged to emissions predominately from the Russian fires. In Figure 11a, data associated with the largest $\Delta^{14}CO_2$ enrichment (262.2‰) observed during ARCTAS are presented. This sample was collected within a huge pollution plume intercepted at 4 km on the 19 April return transit flight. Large enhancements in the combustion tracers CO_2 (396.2 ppmv) and CO (387 ppbv), along with a commensurate increase in CH_3CN (680 pptv), the highest CH_3CN concentration observed during the spring campaign, strongly support the sampling of BB emissions. C_2Cl_4 was only moderately enhanced (4%) within the plume, and the O_3/CO ratio or stratospheric air indicator was quite low (<0.4). The CO_2:CO enhancement ratio was 26.2 ± 1.2, R^2 = 0.88. The emissions sampled had multiple origins, the air parcel coming in contact with the BL as it traveled over Europe and fires in Northeast China and Russia with subsequent lofting to the middle troposphere five days prior to collection (Figure 11b). The highly elevated CO_2, CH_3CN, and CO mixing ratios suggest that the enrichment in $\Delta^{14}CO_2$ resulted from the combustion of older carbon (C) rather than from biospheric respiration or cosmogenic production.

[43] Atmospheric $\Delta^{14}CO_2$ due to past atmospheric nuclear testing reached its peak at about 900‰ in 1964 before declining to levels of about 95‰ in 1999 [*Levin and Hesshaimer*, 2000]. The remobilization of radionuclides by fire and their subsequent inter and intracontinental transport has been previously reported [*Amiro et al.*, 1996; *Wotawa et al.*, 2006], as well as their persistence in high northern ecosystems due to slower turnover rates [*Paliouris et al.*, 1995]. Moreover, $\Delta^{14}CO_2$ values ranging between 110 and 350‰ were reported from an experimental forest fire near Fairbanks, Alaska [*Schuur et al.*, 2003] so it is not unreasonable to attribute the 262.2‰ sample to the release of ^{14}C-enhanced carbon from bomb ^{14}C sequestered in plant carbon pools by boreal wildfires. Given that 77% of the $\Delta^{14}CO_2$ samples were obtained in plumes transported to the study region from the northern midlatitudes yet exhibited little fossil fuel CO_2 influence, the question arises if old C resuspended by biomass burning played a larger role than respiration in offsetting the depletion of $\Delta^{14}CO_2$ by fossil fuels during this high fire season.

[44] For summer, we turn our focus to ten whole air samples collected below 2 km in fresh emissions from Canadian boreal forest fires (Figure 10b). These samples comprise 38% of the overall summer $\Delta^{14}CO_2$ data set (n = 26). Within this subset of data, $\Delta^{14}CO_2$ was enriched (51.8 to 102.2‰) in 90% of the samples, and displayed a positive disequilibrium (i.e., biosphere-atmosphere) of 1–7‰ for values within 2σ of the July clean air maximum value (51.1‰). Within the free troposphere, four samples were enriched in $\Delta^{14}CO_2$ (54.1, 57.6, 55.8, 54.6‰); half the sample number observed in spring. These samples were collected above 5 km, and contained CO_2 and CO enhancements to varying degrees. Three were captured over the Canadian sub-Arctic while the fourth was collected near Alert (ALT) (Figure 10b). Contrary to the spring observations, C_2Cl_4 mixing ratios were not elevated in any of the samples. Overall, the $\Delta^{14}CO_2$ data display a positive disequilibrium comparable to the fresh fire emission values.

[45] ARCTAS-B $\Delta^{14}CO_2$ distributions (Figure 10a) also follow a similar pattern in terms of the low number of samples indicating the addition of fossil fuel CO_2 (n = 2), and in the presence of $\geq 2\sigma$ outliers. These findings are associated with grab samples collected over the Alberta Tar Sands oil recovery operations near Fort McMurray in NE Alberta, and from wildfires near Lake Athabasca, in NW Saskatchewan. One hertz CO_2 and CO data recorded during the filling of four canister samples are presented in Figure 12.

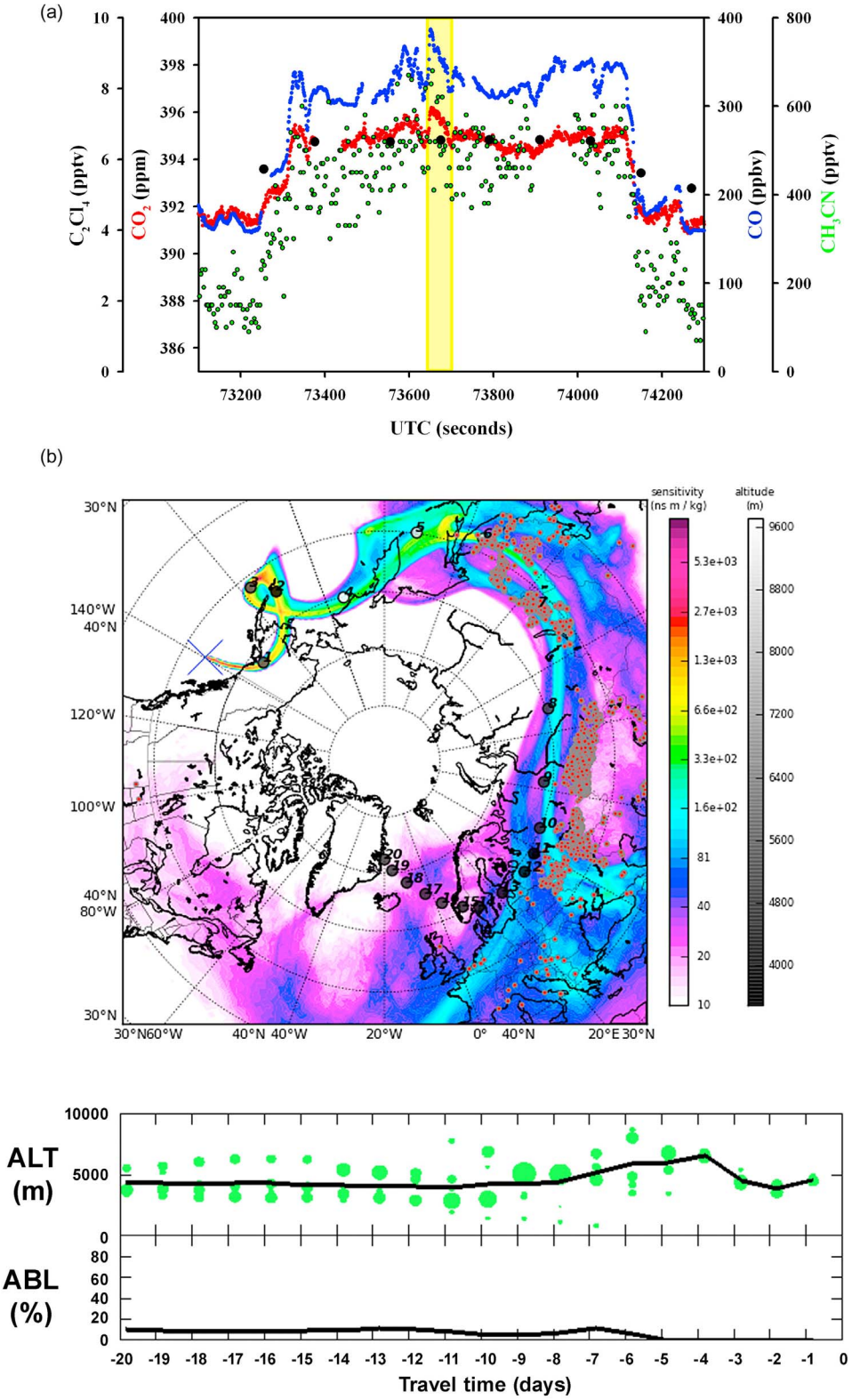

Figure 11. (a) Time series of CO_2, CO, CH_3CN, and C_2Cl_4 during a pollution event sampled on 19 April 2008. Data associated with the 262‰ $\Delta^{14}CO_2$ sample within the shaded region. (b) Same as Figure 7 but for the air parcel containing 262‰ $\Delta^{14}CO_2$.

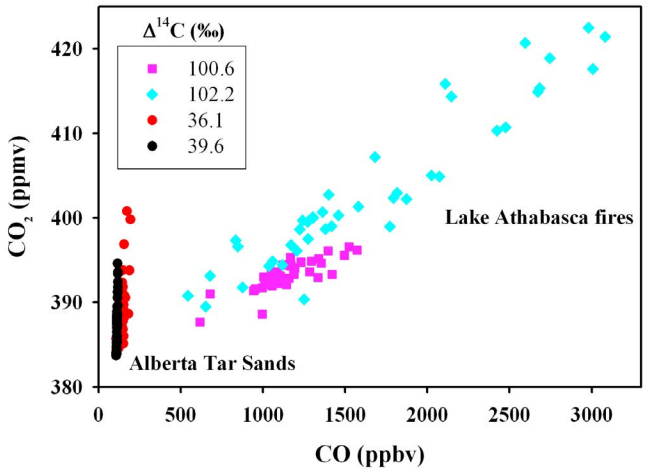

Figure 12. One second CO_2 and CO data recorded during the filling of four individual canisters for radiocarbon analysis. Summertime $\Delta^{14}CO_2$ data reveal a fossil fuel contribution to total measured CO_2 from observations over the Alberta Tar Sands and indicate the resuspension of radionuclides from the combustion of contaminated biomass in the Lake Athabasca fires.

Data collected over the Alberta Tar Sands at 0.8 km show CO_2 rich emissions accompanied by depleted $\Delta^{14}CO_2$ (39.6 and 36.1‰) with minor CO enhancements.

[46] Emissions from the Lake Athabasca fires contained anomalously enriched $\Delta^{14}CO_2$ associated with large CO_2 and CO enhancements clearly related (Figure 12). The CO_2:CO emission ratios in these two plumes were 12.5 ppmv ppmv^{-1} (r^2 = 0.90, 102.2‰), and 7.6 ppmv ppmv^{-1} (r^2 = 0.70, 100.6‰). Concurrent CH_3CN mixing ratios were in excess of 2 ppbv, a definitive fire signature substantiating the addition of CO_2 as a biomass combustion byproduct. As mentioned previously, a plausible source for these high excursions is enrichment due to the resuspension of bomb carbon (^{14}C) in contaminated biomass or soil organic matter due to wildfires [*Schuur et al.*, 2003]. The ^{14}C signature in the four anonymously enriched ARCTAS samples (100.6, 102.2, 112.9, 262.2‰) indicates that the carbon released by fire was stored in respective ecosystems twenty or more years ago.

[47] *Levin et al.* [2010] recently reported that fossil fuel CO_2 emissions remain the only major driver of the north-south $\Delta^{14}CO_2$ gradient today yet found that the sum of all processes contributing to the simulated north-south $\Delta^{14}CO_2$ difference did not exactly match the observed difference which may indicate some missing processes; possibly unaccounted $\Delta^{14}CO_2$ sources in the north. As a result, neither the observed temporal trend nor the north-south $\Delta^{14}CO_2$ gradient may constrain global fossil fuel CO_2 emissions to better than 25%, due to the large uncertainties in these missing components of the radiocarbon cycle [*Levin et al.*, 2010]. The ARCTAS observations clearly show the release of old carbon from boreal ecosystems disturbed by fire as a source of $\Delta^{14}CO_2$ enrichment. With the increase in fire frequency and severity accompanying high-latitude warming, this source then becomes an increasingly important contributor to the mass excess in $\Delta^{14}CO_2$ observations. When unaccounted for or underestimated, the process apparent in the ARCTAS observations represents an additional source of uncertainty in the quantification of fossil fuel CO_2.

6. Conclusions

[48] In the framework of the ARCTAS/POLARCAT experiments, highly precise measurements of atmospheric CO_2 were made from the NASA DC-8 over a significant portion of the North American Arctic and sub-Arctic in spring (4–17 April) and summer (29 June to 10 July) of 2008. Variations in CO_2 were characterized using coincident gas phase and aerosol data, while influential source regions were investigated with the Lagrangian Particle Dispersion Model, FLEXPART. In spring, we found that pollution originating primarily from Eurasian sources provided significant input to the region, leading to enhanced CO_2 mixing ratios in the free troposphere. Sources of the widespread pollution were mainly traced to boreal forest and agricultural residue fires; and Asian urban/industrial sources, the emissions of which were most pronounced above 6.5 km. Local boreal wildfires represented a major source for CO_2 in the sub-Arctic during summer, and were found to emit 1698 ± 280 g kg^{-1} dry matter (DM) on average with a median value of 1634 g kg^{-1} DM. Enhancement ratios determined for CO_2 relative to CO ranged from 27 to 83 ppmv ppmv^{-1} in discrete plumes sampled north of 60°N in spring, and 4 to 16 ppmv ppmv^{-1} in fresh boreal wildfire fire emissions in summer. The overall radiocarbon data set exhibited a negligible fossil fuel CO_2 signature; depleted $\Delta^{14}C$ values were mostly from local sources. The pervasive influence of emissions from fires in the boreal zone complicated the parsing of biogenic and fossil fuel contributions to total measured CO_2 using $\Delta^{14}CO_2$ observations, likely offsetting the fossil fuel CO_2 signal and highlighting some of the uncertainties in using the isotope-based approach for accurate quantification of fossil fuel CO_2.

[49] The ARCTAS campaign provided a unique and extensive body of data from high northern latitudes that is useful for model simulations and space-based retrieval evaluation. The rich data set, collected during the 2007–2008 International Polar Year, is of historical value as a baseline from which to assess future emission changes. ARCTAS data are publicly available at http://www-air.larc.nasa.gov/missions/arctas/arctas.html.

[50] **Acknowledgments.** The authors wish to thank Xiaomei Xu, Scott Lehman, and Ingeborg Levin for use of the Point Barrow, Niwot Ridge, and Jungfraujoch $\Delta^{14}CO_2$ data, respectively. We also appreciate the CO_2 data provided by Doug Worthy of Environment Canada and NOAA ESRL, as well as contributions from Melissa Yang. We are most grateful to Jimmy Geiger, Jim Plant, and the DC-8 crew whose valuable contributions ensured a successful and safe mission. This research was funded by NASA's Global Tropospheric Chemistry and Radiation Sciences Programs. CH_3CN measurements were supported by the Austrian Research Promotion Agency (FFG-ALR) and the Tiroler Zukunftstiftung, and carried out with the help/support of T. Mikoviny, M. Graus, A. Hansel, and T. D. Maerk.

References

Akagi, S. K., et al. (2011), Emission factors for open and domestic biomass burning for use in atmospheric models, *Atmos. Chem. Phys.*, *11*, 4039–4072, doi:10.5194/acp-11-4039-2011.

Alvarado, M. J., et al. (2010), Nitrogen oxides and PAN in plumes from boreal fires during ARCTAS-B and their impact on ozone: An integrated analysis of aircraft and satellite observations, *Atmos. Chem. Phys.*, *10*, 9739–9760, doi:10.5194/acp-10-9739-2010.

Amiro, B. D., S. C. Sheppard, F. L. Johnston, W. G. Evenden, and D. R. Harris (1996), Burning radionuclide question: What happens to iodine, cesium, and chlorine in biomass fires?, *Sci. Total Environ.*, *187*, 93–103, doi:10.1016/0048-9697(96)05125-X.

Barletta, B., et al. (2009), Characterization of volatile organic compounds (VOCs) in Asian and north American pollution plumes during INTEX-B: Identification of specific Chinese air mass tracers, *Atmos. Chem. Phys.*, *9*, 5371–5388, doi:10.5194/acp-9-5371-2009.

Barrie, L. A. (1986), Arctic air pollution: An overview of current knowledge, *Atmos. Environ.*, *20*(4), 643–663, doi:10.1016/0004-6981(86)90180-0.

Blake, D. R., and F. S. Rowland (1995), Urban leakage of liquefied petroleum gas and its impact on Mexico City air quality, *Science*, *269*, 953–956, doi:10.1126/science.269.5226.953.

Blake, D. R., T.-Y. Chen, T. W. Smith Jr., C. J.-L. Wang, O. W. Wingenter, N. J. Blake, and F. S. Rowland (1996), Three-dimensional distribution of nonmethane hydrocarbons and halocarbons over the northwestern Pacific during the 1991 Pacific Exploratory Mission (PEM-West A), *J. Geophys. Res.*, *101*(D1), 1763–1778, doi:10.1029/95JD02707.

Blake, N. J., D. R. Blake, T.-Y. Chen, J. E. Collins Jr., G. W. Sachse, B. E. Anderson, and F. S. Rowland (1997), Distribution and seasonality of selected hydrocarbons and halocarbons over the western Pacific basin during PEM-West A and PEM-West B, *J. Geophys. Res.*, *102*(D23), 28,315–28,331, doi:10.1029/97JD02538.

Blake, N. J., et al. (2003), NMHCs and halocarbons in Asian continental outflow during the transport and chemical evolution over the Pacific (TRACE-P) field campaign: Comparison with PEM-West, *J. Geophys. Res.*, *108*(D20), 8806, doi:10.1029/2002JD003367.

Boggs, P. T., C. H. Spiegelman, J. R. Donaldson, and R. B. Schnabel (1988), A computational examination of orthogonal distance regression, *J. Econometrics*, *38*, 169–201, doi:10.1016/0304-4076(88)90032-2.

Campbell, J. E., et al. (2007), Analysis of anthropogenic CO_2 signal in ICARTT using a regional chemical transport model and observed tracers, *Tellus, Ser. B*, *59*, 199–210.

Choi, Y., et al. (2008), Characteristics of the atmospheric CO_2 signal as observed over the conterminous United States during INTEX-NA, *J. Geophys. Res.*, *113*, D07301, doi:10.1029/2007JD008899.

Crounse, J. D., et al. (2009), Biomass burning and urban air pollution over the Central Mexican Plateau, *Atmos. Chem. Phys.*, *9*, 4929–4944, doi:10.5194/acp-9-4929-2009.

Crutzen, P. J., and M. O. Andreae (1990), Biomass burning in the tropics: Impact on atmospheric chemistry and biogeochemical cycles, *Science*, *250*, 1669–1678, doi:10.1126/science.250.4988.1669.

de Gouw, J. A., C. Warneke, D. D. Parrish, J. S. Holloway, M. Trainer, and F. C. Fehsenfeld (2003), Emission sources and ocean uptake of acetonitrile (CH_3CN) in the atmosphere, *J. Geophys. Res.*, *108*(D11), 4329, doi:10.1029/2002JD002897.

de Gouw, J. A., et al. (2004), Chemical composition of air masses transported from Asia to the U.S. West Coast during ITCT 2K2: Fossil fuel combustion versus biomass-burning signatures, *J. Geophys. Res.*, *109*, D23S20, doi:10.1029/2003JD004202.

de Gouw, J. A., et al. (2006), Volatile organic compounds compositions of merged and aged forest fire plumes from Alaska and western Canada, *J. Geophys. Res.*, *111*, D10303, doi:10.1029/2005JD006175.

Djuricin, S., D. E. Pataki, and X. Xu (2010), A comparison of tracer methods for quantifying CO_2 sources in an urban region, *J. Geophys. Res.*, *115*, D11303, doi:10.1029/2009JD012236.

Fisher, J. A., et al. (2010), Source attribution and interannual variability of Arctic pollution in spring constrained by aircraft (ARCTAS, ARCPAC) and satellite (AIRS) observations of carbon monoxide, *Atmos. Chem. Phys.*, *10*, 977–996, doi:10.5194/acp-10-977-2010.

Fritz, S., et al. (2003), Harmonisation, mosaicing and production of the Global Land Cover 2000 database (Beta version), *EUR 20849 EN*, 41 pp., Off. for Off. Publ. of the Eur. Commun., Luxembourg.

Fuelberg, H. E., D. L. Harrigan, and W. Sessions (2010), A meteorological overview of the ARCTAS 2008 mission, *Atmos. Chem. Phys.*, *10*, 817–842, doi:10.5194/acp-10-817-2010.

Gamnitzer, U., U. Karstens, B. Kromer, R. E. M. Neubert, H. A. J. Meijer, H. Schroeder, and I. Levin (2006), Carbon monoxide: A quantitative tracer for fossil fuel CO_2?, *J. Geophys. Res.*, *111*, D22302, doi:10.1029/2005JD006966.

Giglio, L., I. Csiszar, and C. O. Justice (2006), Global distribution and seasonality of active fires as observed with the Terra and Aqua MODIS sensors, *J. Geophys. Res.*, *111*, G02016, doi:10.1029/2005JG000142.

Goode, J. G., R. J. Yokelson, D. E. Ward, R. A. Susott, R. E. Babbitt, M. A. Davies, and W. M. Hao (2000), Measurements of excess O_3, CO_2, CO, CH_4, C_2H_4, C_2H_2, HCN, NO, NH_3, HCOOH, CH_3COOH, HCHO, and CH_3OH in 1997 Alaskan biomass burning plumes by airborne Fourier transform infrared spectroscopy (AFTIR), *J. Geophys. Res.*, *105*(D17), 22,147–22,166, doi:10.1029/2000JD900287.

Graven, H. D., et al. (2009), Vertical profiles of biospheric and fossil fuel-derived CO_2 and fossil fuel CO_2:CO ratios from airborne measurements of $\Delta^{14}C$, CO_2, and CO above Colorado, USA, *Tellus, Ser. B*, *61*, 536–546.

Gregory, G. L., et al. (1992), Tropospheric ozone and aerosol observations: The Alaskan Arctic, *J. Geophys. Res.*, *97*(D15), 16,451–16,471, doi:10.1029/91JD01310.

Hansen, D. A., and T. Novakov (1989), Real time measurement of the size fractionation of ambient black carbon aerosols at elevated humidities, *Aerosol Sci. Technol.*, *10*, 106–110, doi:10.1080/02786828908959225.

Harrigan, D. L., et al. (2011), Transport of anthropogenic emissions during ARCTAS-A: A climatology and regional case studies, *Atmos. Chem. Phys. Discuss.*, *11*, 5435–5491, doi:10.5194/acpd-11-5435-2011.

Heald, C. L., et al. (2003), Asian outflow and trans-Pacific transport of carbon monoxide and ozone pollution: An integrated satellite, aircraft, and model perspective, *J. Geophys. Res.*, *108*(D24), 4804, doi:10.1029/2003JD003507.

Heard, D. E., L. J. Carpenter, D. J. Creasey, J. R. Hopkins, J. D. Lee, A. C. Lewis, M. J. Pilling, P. W. Seakins, N. Carslaw, and K. M. Emmerson (2004), High levels of the hydroxyl radical in the winter urban troposphere, *Geophys. Res. Lett.*, *31*, L18112, doi:10.1029/2004GL020544.

Hegg, D. A., L. F. Radke, P. V. Hobbs, R. A. Rasmussen, and P. J. Riggan (1990), Emissions of some trace gases from some biomass fires, *J. Geophys. Res.*, *95*(D5), 5669–5675, doi:10.1029/JD095iD05p05669.

Higuchi, K., D. Worthy, D. Chan, and A. Shashkov (2003), Regional source/sink impact on the diurnal, seasonal and inter-annual variations in atmospheric CO_2 at a boreal forest site in Canada, *Tellus, Ser. B*, *55*, 115–125.

Hsueh, D. Y., N. Y. Krakauer, J. T. Randerson, X. Xu, S. E. Trumbore, and J. R. Southon (2007), Regional patterns of radiocarbon and fossil fuel derived CO_2 in surface air across North America, *Geophys. Res. Lett.*, *34*, L02816, doi:10.1029/2006GL027032.

Hudman, R. C., et al. (2007), Surface and lightning sources of nitrogen oxides over the United States: Magnitudes, chemical evolution, and outflow, *J. Geophys. Res.*, *112*, D12S05, doi:10.1029/2006JD007912.

Jacob, D. J., et al. (2010), The Arctic Research of the Composition of the Troposphere from Aircraft and Satellites (ARCTAS) mission: Design, execution, and first results, *Atmos. Chem. Phys.*, *10*, 5191–5212, doi:10.5194/acp-10-5191-2010.

Kasischke, E. S., and L. P. Bruhwiler (2002), Emissions of carbon dioxide, carbon monoxide, and methane from boreal forest fires in 1998, *J. Geophys. Res.*, *107*, 8146, doi:10.1029/2001JD000461 [printed *108*(D1), 2003].

Kasischke, E. S., E. J. Hyer, P. C. Novelli, L. P. Bruhwiler, N. H. F. French, A. I. Sukhinin, J. H. Hewson, and B. J. Stocks (2005), Influences of boreal fire emissions on Northern Hemisphere atmospheric carbon and carbon monoxide, *Global Biogeochem. Cycles*, *19*, GB1012, doi:10.1029/2004GB002300.

Katzenstein, A. S., et al. (2003), Extensive regional atmospheric hydrocarbon pollution in the Southwestern United States, *Proc. Natl. Acad. Sci. U. S. A.*, *100*, 11,975–11,979, doi:10.1073/pnas.1635258100.

Klonecki, A., P. Hess, L. Emmons, L. Smith, J. Orlando, and D. Blake (2003), Seasonal changes in the transport of pollutants into the Arctic troposphere-model study, *J. Geophys. Res.*, *108*(D4), 8367, doi:10.1029/2002JD002199.

Koch, D., and J. Hansen (2005), Distant origins of Arctic black carbon: A Goddard Institute for Space Studies ModelE experiment, *J. Geophys. Res.*, *110*, D04204, doi:10.1029/2004JD005296.

Kondo, Y., et al. (2011), Emissions of black carbon, organic, and inorganic aerosols from biomass burning in North America and Asia in 2008, *J. Geophys. Res.*, *116*, D08204, doi:10.1029/2010JD015152.

Law, K. S., and A. Stohl (2007), Arctic air pollution: Origins and impacts, *Science*, *315*, 1537–1540, doi:10.1126/science.1137695.

Lefer, B. L., et al. (1994), Enhancement of acidic gases in biomass burning impacted air masses over Canada, *J. Geophys. Res.*, *99*(D1), 1721–1737, doi:10.1029/93JD02091.

Levin, I., and V. Hesshaimer (2000), Radiocarbon—A unique tracer of global carbon cycle dynamics, *Radiocarbon*, *42*(1), 69–80.

Levin, I., K. O. Munnich, and W. Weiss (1980), The effect of anthropogenic CO_2 and ^{14}C sources on the distribution of ^{14}C in the atmosphere, *Radiocarbon*, *22*(2), 379–391.

Levin, I., et al. (2010), Observations and modelling of the global distribution and long-term trend of atmospheric $^{14}CO_2$, *Tellus, Ser. B*, *62*, 26–46, doi:10.1111/j.1600-0889.2009.00446.x.

Li, Q., D. J. Jacob, I. Bey, R. M. Yantosca, Y. Zhao, Y. Kondo, and J. Notholt (2000), Atmospheric hydrogen cyanide (HCN): Biomass burning source, ocean sink? *Geophys. Res. Lett.*, *27*(3), 357–360, doi:10.1029/1999GL010935.

Li, Q., D. J. Jacob, R. M. Yantosca, C. L. Heald, H. B. Singh, M. Koike, Y. Zhao, G. W. Sachse, and D. G. Streets (2003), A global three-dimensional model analysis of the atmospheric budgets of HCN and CH_3CN: Constraints from aircraft and ground measurements, *J. Geophys. Res.*, *108*(D21), 8827, doi:10.1029/2002JD003075.

Liu, H., D. J. Jacob, I. Bey, R. M. Yantosca, B. N. Duncan, and G. W. Sachse (2003), Transport pathways for Asian pollution outflow over the Pacific: Interannual and seasonal variations, *J. Geophys. Res.*, *108*(D20), 8786, doi:10.1029/2002JD003102.

Matsui, H., et al. (2011), Seasonal variation of the transport of black carbon aerosol from the Asian continent to the Arctic during the ARCTAS aircraft campaign, *J. Geophys. Res.*, *116*, D05202, doi:10.1029/2010JD015067.

Moteki, N., and Y. Kondo (2007), Effects of mixing state on black carbon measurements by laser-induced incandescence, *Aerosol Sci. Technol.*, *41*, 398–417, doi:10.1080/02786820701199728.

Naegler, T., and I. Levin (2009), Biosphere-atmosphere gross carbon exchange flux and the $\delta^{13}CO_2$ and $\Delta^{14}CO_2$ disequilibria constrained by the biospheric excess radiocarbon inventory, *J. Geophys. Res.*, *114*, D17303, doi:10.1029/2008JD011116.

Newman, S., X. Xu, H. P. Affek, E. Stolper, and S. Epstein (2008), Changes in mixing ratio and isotopic composition of CO_2 in urban air from the Los Angeles basin, California, between 1972 and 2003, *J. Geophys. Res.*, *113*, D23304, doi:10.1029/2008JD009999.

Oechel, W. C., and G. L. Vourlitis (1994), The effects of climate change on Arctic tundra ecosystems, *Trends Ecol. Evol.*, *9*, 324–329, doi:10.1016/0169-5347(94)90152-X.

Paliouris, G., H. W. Taylor, R. W. Wein, J. Svoboda, and B. Mierzynski (1995), Fire as an agent in redistributing fallout ^{137}Cs in the Canadian boreal forest, *Sci. Total Environ.*, *160–161*, 153–166, doi:10.1016/0048-9697(95)04353-3.

Paris, J.-D., et al. (2009), Wildfire smoke in the Siberican Arctic in summer: Source characterization and plume evolution from airborne measurements, *Atmos. Chem. Phys.*, *9*, 9315–9327, doi:10.5194/acp-9-9315-2009.

Pataki, D. E., D. R. Bowling, and J. R. Ehleringer (2003), Seasonal cycle of carbon dioxide and its isotopic composition in an urban atmosphere: Anthropogenic and biogenic effects, *J. Geophys. Res.*, *108*(D23), 4735, doi:10.1029/2003JD003865.

Peischl, J., et al. (2010), A top-down analysis of emissions from selected Texas power plants during TexAQS 2000 and 2006, *J. Geophys. Res.*, *115*, D16303, doi:10.1029/2009JD013527.

Quinn, P. K., et al. (2007), Arctic haze: Current trends and knowledge gaps, *Tellus, Ser. B*, *59*, 99–114.

Randerson, J. T., I. G. Enting, E. A. G. Schuur, K. Caldeira, and I. Y. Fung (2002), Seasonal and latitudinal variability of troposphere $\Delta^{14}CO_2$: Post bomb contributions from fossil fuels, oceans, the stratosphere, and the terrestrial biosphere, *Global Biogeochem. Cycles*, *16*(4), 1112, doi:10.1029/2002GB001876.

Rastigejev, Y., R. Park, M. P. Brenner, and D. J. Jacob (2010), Resolving intercontinental pollution plumes in global models of atmospheric transport, *J. Geophys. Res.*, *115*, D02302, doi:10.1029/2009JD012568.

Sachse, G. W., G. F. Hill, L. O. Wade, and M. G. Perry (1987), Fast-response, high-precision carbon monoxide sensor using a tunable diode laser absorption technique, *J. Geophys. Res.*, *92*(D2), 2071–2081, doi:10.1029/JD092iD02p02071.

Saha, A., et al. (2010), Pan-Arctic sunphotometry during the ARCTAS-A campaign of April 2008, *Geophys. Res. Lett.*, *37*, L05803, doi:10.1029/2009GL041375.

Schuur, E. A. G., S. E. Trumbore, M. C. Mack, and J. W. Harden (2003), Isotopic composition of carbon dioxide from a boreal forest fire: Inferring carbon loss from measurements and modeling, *Global Biogeochem. Cycles*, *17*(1), 1001, doi:10.1029/2001GB001840.

Shindell, D. T., et al. (2008), A multi-model assessment of pollutant transport to the Arctic, *Atmos. Chem. Phys.*, *8*, 5353–5372, doi:10.5194/acp-8-5353-2008.

Simpson, I. J., et al. (2010), Characterization of trace gases measured over Alberta oil sands mining operations: 75 speciated C_2-C_{10} volatile organic compounds (VOCs), CO_2, CO, CH_4, NO, NO_y, O_3 and SO_2, *Atmos. Chem. Phys.*, *10*, 11,931–11,954, doi:10.5194/acp-10-11931-2010.

Simpson, I. J., et al. (2011), Boreal forest fire emissions in fresh Canadian smoke plumes:C_1-C_{10} volatile organic compounds (VOCs), CO_2, CO, NO_2, NO, HCN and CH_3CN, *Atmos. Chem. Phys. Discuss.*, *11*, 9515–9566, doi:10.5194/acpd-11-9515-2011.

Soja, A. J., W. R. Cofer, H. H. Shugart, A. I. Sukhinin, P. W. Stackhouse Jr., D. J. McRae, and S. G. Conard (2004), Estimating fire emissions and disparities in boreal Siberia (1998–2002), *J. Geophys. Res.*, *109*, D14S06, doi:10.1029/2004JD004570.

Soja, A. J., B. Stocks, P. Maczeck, M. Fromm, R. Servranckx, M. Turetsky, and B. Benscoter (2008), ARCTAS: The perfect smoke, *Can. Smoke Newsl.*, Fall 2008, 2–7.

Staudt, A. C., D. J. Jacob, J. A. Logan, D. Bachiochi, T. N. Krishnamurti, and G. W. Sachse (2001), Continental sources, transoceanic transport, and interhemispheric exchange of carbon monoxide over the Pacific, *J. Geophys. Res.*, *106*(D23), 32,571–32,589, doi:10.1029/2001JD900078.

Stocks, B. J. (1991), The extent and impact of forest fires in northern circumpolar countries, in *Global Biomass Burning: Atmospheric, Climatic, and Biospheric Implications*, edited by J. S. Levine, pp. 197–202, MIT Press, Cambridge, Mass.

Stocks, B. J., et al. (1998), Climate change and forest fire potential in Russian and Canadian boreal forests, *Clim. Change*, *38*, 1–13, doi:10.1023/A:1005306001055.

Stohl, A. (2006), Characteristics of atmospheric transport into the Arctic troposphere, *J. Geophys. Res.*, *111*, D11306, doi:10.1029/2005JD006888.

Stohl, A., S. Eckhardt, C. Forster, P. James, N. Spichtinger, and P. Seibert (2002), A replacement for simple back trajectory calculations in the interpretation of atmospheric trace substance measurements, *Atmos. Environ.*, *36*(29), 4635–4648, doi:10.1016/S1352-2310(02)00416-8.

Stuiver, M., and H. A. Polach (1977), Reporting of ^{14}C data, *Radiocarbon*, *19*(3), 355–363.

Suess, H. E. (1955), Radiocarbon concentration in modern wood, *Science*, *122*, 415–417, doi:10.1126/science.122.3166.415-a.

Suntharalingam, P., et al. (2004), Improved quantification of Chinese carbon fluxes using CO_2/CO correlations in Asian outflow, *J. Geophys. Res.*, *109*, D18S18, doi:10.1029/2003JD004362.

Susott, R. A., G. J. Olbu, S. P. Baker, D. E. Ward, J. B. Kauffman, and R. W. Shea (1996), Carbon, hydrogen, nitrogen, and thermogravimetric analysis of tropical ecosystem biomass, in *Biomass Burning and Global Change*, edited by J. S. Levine, pp. 350–360, MIT Press, Cambridge, Mass.

Turnbull, J. C., J. B. Miller, S. J. Lehman, P. P. Tans, R. J. Sparks, and J. Southon (2006), Comparison of $^{14}CO_2$, CO, and SF_6 as tracers for recently added fossil fuel CO_2 in the atmosphere and implications for biological CO_2 exchange, *Geophys. Res. Lett.*, *33*, L01817, doi:10.1029/2005GL024213.

Turnbull, J., P. Rayner, J. Miller, T. Naegler, P. Ciais, and A. Cozic (2009), On the use of $^{14}CO_2$ as a tracer for fossil fuel CO_2: Quantifying uncertainties using an atmospheric transport model, *J. Geophys. Res.*, *114*, D22302, doi:10.1029/2009JD012308.

Tyler, S. C., H. O. Ajie, M. L. Gupta, R. J. Cicerone, D. R. Blake, and E. J. Dlugokencky (1999), Carbon isotopic composition of atmospheric methane: A comparison of surface level and upper tropospheric air, *J. Geophys. Res.*, *104*(D11), 13,895–13,910, doi:10.1029/1999JD900029.

Vay, S. A., B. E. Anderson, T. J. Conway, G. W. Sachse, J. E. Collins Jr., D. R. Blake, and D. J. Westberg (1999), Airborne observations of the tropospheric CO_2 distribution and its controlling factors over the south Pacific Basin, *J. Geophys. Res.*, *104*(D5), 5663–5676, doi:10.1029/98JD01420.

Vay, S. A., et al. (2003), Influence of regional-scale anthropogenic emissions on CO_2 distributions over the western North Pacific, *J. Geophys. Res.*, *108*(D20), 8801, doi:10.1029/2002JD003094.

Vay, S. A., et al. (2009), Sources and transport of $\Delta^{14}C$ in CO_2 within the Mexico City Basin and vicinity, *Atmos. Chem. Phys.*, *9*, 4973–4985, doi:10.5194/acp-9-4973-2009.

Vogel, F. R., et al. (2010), Implication of weekly and diurnal ^{14}C calibration on hourly estimates of CO-based fossil fuel CO_2 at a moderately polluted site in southwestern Germany, *Tellus, Ser. B*, *62*, 512–520.

Wang, Y., J. W. Munger, S. Xu, M. B. McElroy, J. Hao, C. P. Nielsen, and H. Ma (2010), CO_2 and its correlation with CO at a rural site near Beijing: Implications for combustion efficiency in China, *Atmos. Chem. Phys.*, *10*, 8881–8897, doi:10.5194/acp-10-8881-2010.

Ward, D. E., and L. F. Radke (1993), Emissions measurements from vegetation fires: A comparative evaluation of methods and results, in *Fire in the Environment: The Ecological, Atmospheric and Climatic Importance of Vegetation Fires*, edited by P. J. Crutzen and J. G. Goldammer, pp. 53–76, John Wiley, Hoboken, N. J.

Warneke, C., et al. (2009), Biomass burning in Siberia and Kazakhstan as an important source for haze over the Alaskan Arctic in April 2008, *Geophys. Res. Lett.*, *36*, L02813, doi:10.1029/2008GL036194.

Weinheimer, A. J., J. G. Walega, B. A. Ridley, B. L. Gary, D. R. Blake, N. J. Blake, F. S. Rowland, G. W. Sachse, B. E. Anderson, and J. E. Collins (1994), Meridional distributions of NO_x, NO_y, and other species in the

lower stratosphere and upper troposphere during AASE II, *Geophys. Res. Lett.*, *21*(23), 2583–2586, doi:10.1029/94GL01897.

Wisthaler, A., A. Hansel, R. R. Dickerson, and P. J. Crutzen (2002), Organic trace gas measurements by PTR-MS during INDOEX 1999, *J. Geophys. Res.*, *107*(D19), 8024, doi:10.1029/2001JD000576.

Witte, J. C., M. R. Schoeberl, A. R. Douglass, J. F. Gleason, N. A. Krotkov, J. C. Gille, K. E. Pickering, and N. Livesey (2009), Satellite observations of changes in air quality during the 2008 Beijing Olympics and Paralympics, *Geophys. Res. Lett.*, *36*, L17803, doi:10.1029/2009GL039236.

Wofsy, S. C., et al. (1992), Atmospheric chemistry in the arctic and subarctic: Influence of natural fires, industrial emissions, and stratospheric inputs, *J. Geophys. Res.*, *97*(D15), 16,731–16,746, doi:10.1029/92JD00622.

Worthy, D. E., E. Chan, M. Ishizawa, D. Chan, C. Poss, E. J. Dlugokencky, S. Maksyutov, and I. Levin (2009), Decreasing anthropogenic methane emissions in Europe and Siberia inferred from continuous carbon dioxide and methane observations at Alert, Canada, *J. Geophys. Res.*, *114*, D10301, doi:10.1029/2008JD011239.

Wotawa, G., L.-E. De Geer, A. Becker, R. D'Amours, M. Jean, R. Servranckx, and K. Ungar (2006), Inter- and intra-continental transport of radioactive cesium released by boreal forest fires, *Geophys. Res. Lett.*, *33*, L12806, doi:10.1029/2006GL026206.

Xu, X., S. Trumbore, H. Ajie, S. Tyler, J. Randerson, and N. Krakauer (2004), Atmospheric $^{14}CO_2$ over the mid Pacific Ocean and at Point Barrow, Alaska, USA from 2002 to 2004, *Eos Trans. AGU*, *85*(47), Fall Meet. Suppl., Abstract B23A-0948.

Yashiro, H., S. Sugawara, K. Sudo, S. Aoki, and T. Nakazawa (2009), Temporal and spatial variations of carbon monoxide over the western part of the Pacific Ocean, *J. Geophys. Res.*, *114*, D08305, doi:10.1029/2008JD010876.

Yokelson, R. J., D. W. T. Griffith, and D. E. Ward (1996), Open-path Fourier transform infrared studies of large-scale laboratory biomass fires, *J. Geophys. Res.*, *101*(D15), 21,067–21,080, doi:10.1029/96JD01800.

J. F. Burkhart and A. Stohl, Norwegian Institute for Air Research, N-2027 Kjeller, Norway.

D. R. Blake, Department of Chemistry, University of California, Irvine, CA 92697, USA.

Y. Choi and G. W. Sachse, National Institute of Aerospace, Hampton, VA 23666, USA.

K. P. Vadrevu, Department of Geography, University of Maryland, College Park, MD 20740, USA.

G. S. Diskin and S. A. Vay, Chemistry and Dynamics Branch, NASA Langley Research Center, Hampton, VA 23681, USA. (Stephanie.A.Vay@nasa.gov)

A. Hecobian, School of Earth and Atmospheric Sciences, Georgia Institute of Technology, Atlanta, GA 30332, USA.

Y. Kondo, Department of Earth and Planetary Science, University of Tokyo, Tokyo 113-0033, Japan.

S. C. Tyler, Chemistry Program, Norco College, Norco CA 92860, USA.

A. J. Weinheimer, Atmospheric Chemistry Division, National Center for Atmospheric Research, Boulder, CO 80307, USA.

P. O. Wennberg, Division of Geological and Planetary Sciences, California Institute of Technology, Pasadena, CA 91125, USA.

A. Wisthaler, Institute for Ion Physics & Applied Physics, University of Innsbruck, A-6020 Innsbruck, Austria.

J.-H. Woo, Department of Advanced Technology Fusion, Konkuk University, Seoul 143 701, South Korea.